ACS OMEGA

http://pubs.acs.org/journal/acsodf

Article

Insights into the Reactivity of the Ring-Opening Reaction of Tetrahydrofuran by Intramolecular Group-13/P- and Al/Group-15-Based Frustrated Lewis Pairs

Zheng-Feng Zhang and Ming-Der Su*

Cite This: *ACS Omega* 2023, 8, 5316−5331

Read Online

ACCESS | Metrics & More | Article Recommendations | Supporting Information

ABSTRACT: A theoretical study concerning key factors affecting activation energies for ring-opening reactions of tetrahydrofuran (THF) by G13/P-based (G13 = B, Al, Ga, In, and Tl) and Al/G15-based (G15 = N, P, As, Sb, and Bi) frustrated Lewis pairs (FLPs) featuring the dimethylxanthene scaffold was performed using density functional theory. Our theoretical findings indicate that only dimethylxanthene backbone **Al/P-Rea** (Rea = reactant) FLP-type molecules can be energetically favorable to undergo the ring-opening reaction with THF. Our theoretical evidence reveals that the shorter the separating distance between Lewis acidic (LA) and Lewis basic (LB) centers of the dimethylxanthene backbone FLP-type molecules, the greater the orbital overlaps between the FLP and THF and the lower the activation barrier for such a ring-opening reaction. Energy decomposition analysis (EDA) evidence suggests that the bonding interaction for such a ring-opening reaction is predominated by the donor−acceptor interaction (singlet−singlet interaction) compared to the electron-sharing interaction (triplet−triplet interaction). In addition, the natural orbitals for chemical valence (NOCV) evidence demonstrate that the bonding situations of such ring-opening reactions can be best described as FLP-to-THF forward bonding (the lone pair (G15) → the empty σ^*(C−O)) and THF-to-FLP back bonding (the empty σ^*(G13) ← filled p-π(O)). The EDA-NOCV observations show that the former plays a predominant role and the latter plays a minor role in such bonding conditions. The activation strain model reveals that the deformation energy of THF is the key factor in determining the activation energy of their ring-opening reactions. Comparing the geometrical structures of the transition states with their corresponding reactants, a linear relationship between them can be rationally explained by the Hammond postulate combined with the respective activation barriers calculated in this work.

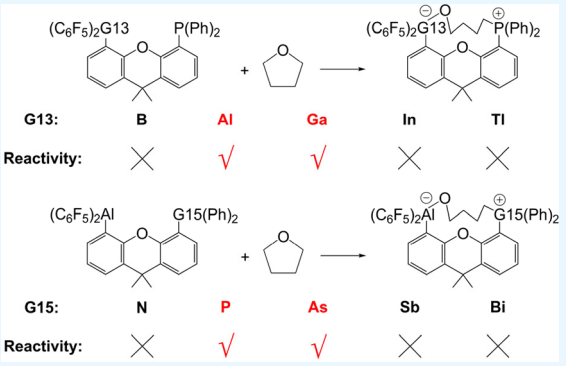

I. INTRODUCTION

Frustrated Lewis pairs (FLPs) are known for their steric bulks, which can sufficiently prevent adduct formation between the Lewis acid (LA) and Lewis base (LB) because of their sterically induced inability to quench one another.[1−3] Since the initial findings by Stephan and co-workers 15 years ago,[1] FLP chemistry has become a powerful strategy to activate small molecules[2−19] and develop reactivity/reaction in laboratories.[20−22] In addition, FLP reactions are widely utilized in modern experiments because the activation of small molecules conventionally requires the participation of transition metals, which are usually expensive and environmentally harmful. By contrast, most FLP reactions do not involve transition-metal-catalyzed processes; thus, metal-free FLPs are suitable for catalysts and activation reactions used under nontoxic conditions.[1−22] After more than 10 years of effort, chemists have discovered that many novel and interesting FLP reactions can be exhibited by combining a variety of inter- and intramolecular LA and LB. Many theoretical studies on FLP-promoted small-molecule activation have been published elsewhere.[23−34] Thus, the FLP chemistry has attracted considerable interest for their use in studying fundamental chemistry problems and for their widespread applications, particularly in heterogeneous catalysis, polymers, solid-state chemistry, and bioorganic and bioinorganic syntheses.[1−22]

Recently, Limberg and co-workers reported that the intramolecular P/Al-based FLP-type molecules featuring the dimethylxanthene backbone can be synthesized, crystallized, and used to activate tetrahydrofuran (THF) to undergo ring-opening reactions (Scheme 1).[35] The intramolecular FLP-type molecule featuring the dimethylxanthene scaffold, in which an LB phosphine center and an LA borane center are compelled with each other in a distance of 4.24 Å,[35] was reported and

Received: September 26, 2022
Accepted: January 12, 2023
Published: January 31, 2023

https://doi.org/10.1021/acsomega.2c06194
ACS Omega 2023, 8, 5316−5331

Scheme 1. Reactions of Dimethylxanthene Backbone Al/P-Based FLP-Type Molecules Containing (a) a $(Mes)_2Al$ and (b) a $(C_6F_5)_2Al$ Site with THF to produce ring-opened products

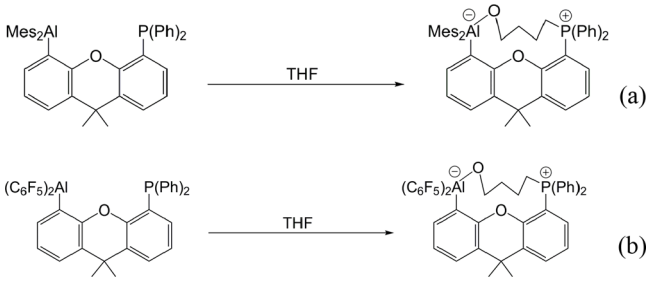

structurally characterized by Aldridge et al. in 2015. Although experimental examples of intermolecular LA-LB-mediated ring-opening reactions of THF have been published elsewhere,[36−42] to the best of our knowledge, only two papers concerning the THF ring-opening reaction by the intramolecular FLP-assisted molecule were reported by Limberg,[35] Wass,[43] and co-workers. Based on available mechanistic studies,[35] THF is initially activated at the LA aluminum element and then attacked by the basic phosphine function. Moreover, Limberg's laboratory has observed that increasing the Lewis acidity of the Al center through C_6F_5 groups can increase the reaction rate by 10-fold compared with Mes substituents.[35] Based on the aforementioned findings, we aim to investigate the reactivity of the ring-opening reaction of THF via an intramolecular G13/G15-based (G13 = B, Al, Ga, In, Tl and G15 = N, P, As, Sb, Bi) FLP-assisted molecule possessing the dimethylxanthene backbone as schematically represented in eqs 1 and 2. In this work, we use

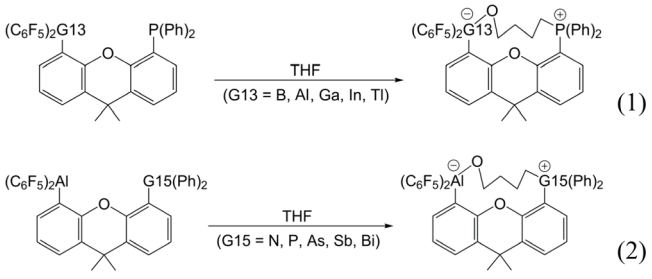

density functional theory (DFT) and several sophisticated theoretical approaches to comprehend the key factors affecting activation barriers and the chemical reactivity trend for the element−substituent effect of the FLP molecule on the THF ring-opening reaction.

II. METHODOLOGY

All of the structures reported in this work were fully optimized without symmetry constraints using the Gaussian 16 program package.[44] Geometry optimizations were conducted using the B3LYP functional.[45,46] The def2-TZVP[47] basis set was used for all atoms. Grimme's dispersion-corrected functional (DFT-3D)[48] with BJ damping[49] was used to account for dispersion interactions. Thus, it was denoted as B3LYP-D3(BJ)/def2-TZVP. We have chosen B3LYP for this project because it gives the agreement of the calculated main-group chemistry and kinetics with the observed data.[50,51] Frequency analysis was performed to verify the characteristics of all optimized structures as minima (the number of imaginary frequencies is zero) or transition states (TSs; the number of imaginary frequencies is one). Transition states were submitted to intrinsic reaction coordinate (IRC)[52] computations to check the energy profiles connecting each TS to two associated minima. Moreover, frequency calculations provide the thermal corrections of the Gibbs free energy (ΔG) at 298.15 K and 1 atm.

The activation strain model (ASM)[53−55] (or distortion/interaction model)[56,57] was used with the Gaussian 16 program package to provide insights into the physical factors controlling the height of the activation barriers and reactivity trends upon changing the structure of the reactants. The activation energy (ΔE_{ACT}) was decomposed into the deformation energy (ΔE_{def}) and interaction energy (ΔE_{INT}) among the deformed reactants,

$$\Delta E_{ACT} = \Delta E_{DEF} + \Delta E_{INT} \quad (3)$$

Furthermore, as shown in eq 4, ΔE_{INT} among reacting species was divided into the electrostatic interaction (ΔE_{Elstat}), Pauli repulsion (ΔE_{Pauli}), orbital interaction (ΔE_{Orb}), and dispersion effect (ΔE_{Disp}) by energy decomposition analysis (EDA)[58−62] based on the Kohn−Sham molecular orbitals.

$$\Delta E_{INT} = \Delta E_{Elstat} + \Delta E_{Pauli} + \Delta E_{Orb} + \Delta E_{Disper} \quad (4)$$

Moreover, the bonding situations in the present FLP system were studied by EDA and the natural orbitals for chemical valence (NOCV)[63−66] method, which can partition the total ΔE_{Orb} term into pairwise contributions of the orbital interactions. Details of the EDA-NOCV[58−66] method, which decomposes the bond energy in several well-defined terms, can be found elsewhere.[67,68] This approach has been proven to be a highly efficient tool for describing the bonding conditions in different types of systems.[69,70] EDA-NOCV computations were thus carried out at the zeroth-order regular approximation ZORA[71]-B3LYP-D3(BJ)/TZ2P[72]//B3LYP-D3(BJ)/def2-TZVP level, where the scalar relativistic effects were included by adopting the ZORA. All EDA-NOCV computations were performed using the Amsterdam density functional[73] program package.

III. THEORETICAL MODEL

Before discussing the computational results of the potential energy profile, the bonding models utilized in this work were explored. Based on previous theoretical analyses,[51] two electronic interaction models can be used to understand the bonding conditions between THF and the G13/G15-assisted FLP-associated molecule. The first model is the donor−acceptor model, which is named the singlet−singlet (S−S) model. The other model is called the electron-sharing interaction model, which is viewed as the triplet−triplet (T-T) model. They are schematically presented in Figure 1(a) and (b), respectively. The former can be written as $[G13/G15]^1 + [THF]^1 \rightarrow [Prod]^1$, and the latter can be described as $[G13/G15]^3 + [THF]^3 \rightarrow [Prod]^1$. Notably, for the latter model, we propose its TS for the ring-opening reaction of THF by G13/G15-FLP, which is composed of the respective triplet states of reactants. Consequently, two individual triplets are coupled to an overall singlet state. The bonding characteristics for the singlet−singlet and triplet−triplet models are similar to those of the Fischer-type[74] and Schrock-type[75] metal carbenes, respectively, which are widely utilized in the field of organometallic chemistry (Figure 2).

https://doi.org/10.1021/acsomega.2c06194
ACS Omega 2023, 8, 5316−5331

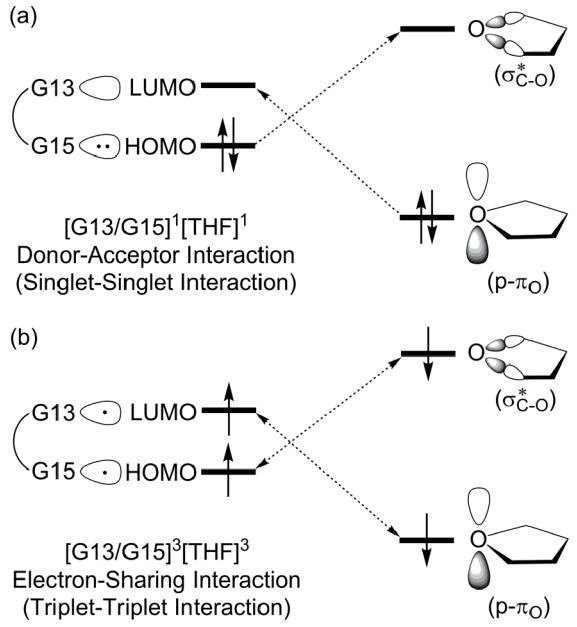

Figure 1. Schematic interaction diagram for (a) the donor−acceptor (or singlet−singlet) model and (b) the electron-sharing (or triplet−triplet) model.

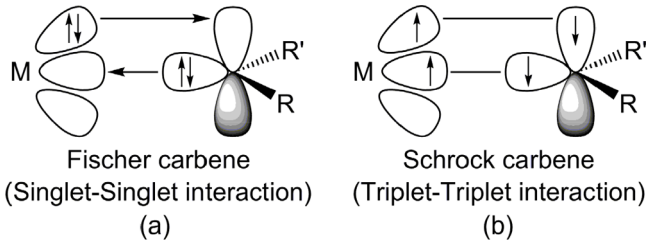

Figure 2. Schematic representations for (a) the Fischer-type metal carbene and (b) the Schrock-type metal carbene.

Scheme 2. (a) Intermediate of the Mes-Substituted Al/P-FLP with THF and (b) Intermediate of the C_6F_5-Substituted Al/P-FLP with THF

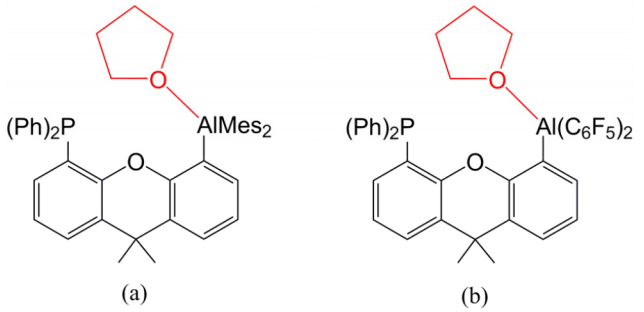

IV. RESULTS AND DISCUSSION

IV.1. Ring-Opening Reactions of THF by G13/P-Based (G13 = Group 13 Element) and Al/G15-Based (G15 = Group 15 Element) FLPs. The calculated results for the four regions on the potential energy profiles of eq 1 are shown in Figure 3: **G13/P-Rea** (Rea = reactant) + THF → **G13/P-PC** (PC = precursor complex)[76] → **G13/P-TS** (TS = transition state) → **G13/P-Prod** (Prod = product). Our theoretical investigations collected in Figure 3 suggest that all five **G13/P-Rea** species have a separating G13(LA)···P(LB) distance (Å),[77] whose order increases in the order **Al/P-Rea** (2.655) < **Ga/P-Rea** (2.731) < **In/P-Rea** (2.819) < **Tl/P-Rea** (3.001) < **B/P-Rea** (4.213). It is noted that our B3LYP evidence reveals that **B/P-Rea** has the largest separating distance between LA and LB in all dimethylxanthene-based **G13/P-Rea** FLPs. Presumably, there may be two reasons for this. One possible reason is that the atomic radius of the B element is the smallest among the group 13 family.[78,79] The other possible reason is that atoms with more electrons have stronger dispersion forces. Hence, the heavy G13′ atom (= Al, Ga, In, and Tl) acting as LA and P acting as LB have a strong attraction so that the separating distance

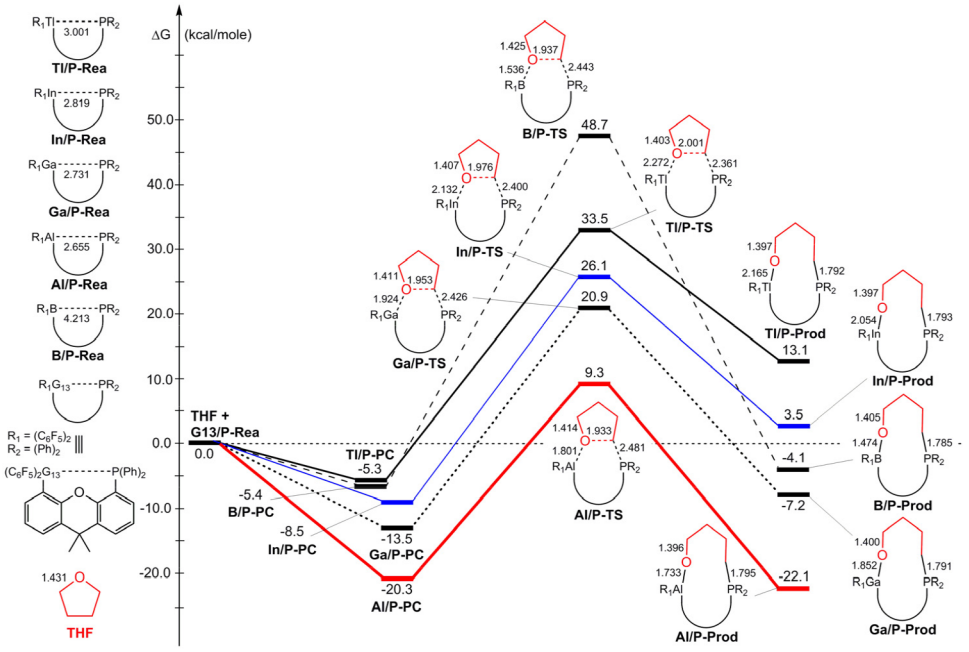

Figure 3. Computed reaction profiles for the ring-opening reaction of dimethylxanthene-based **G13/P-Rea** with THF at the B3LYP-D3(BJ)/def2-TZVP level. Relative free energies and bond lengths are given in kcal/mol and angstroms, respectively.

https://doi.org/10.1021/acsomega.2c06194
ACS Omega 2023, 8, 5316−5331

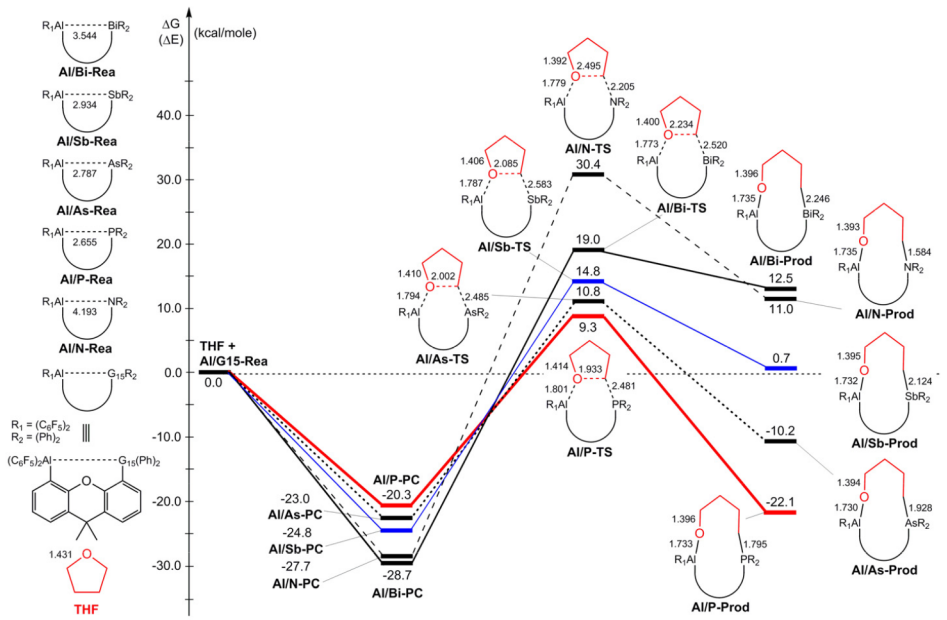

Figure 4. Computed reaction profiles for the ring-opening reaction of dimethylxanthene-based **Al/G15-Rea** with THF at the B3LYP-D3(BJ)/def2-TZVP level. Relative free energies and bond lengths are given in kcal/mol and angstroms, respectively.

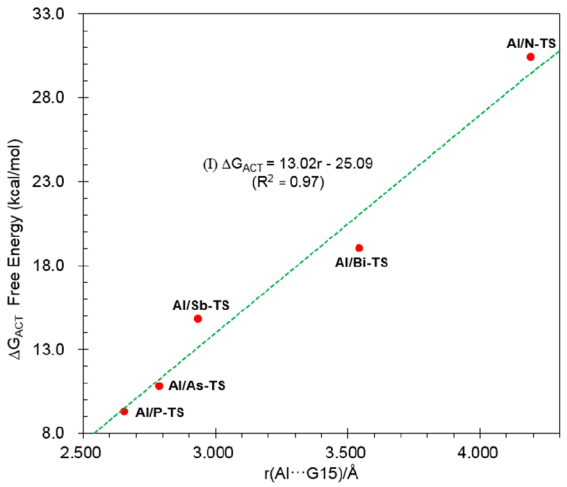

Figure 5. Plot of the free activation energy (ΔG_{ACT}) vs the Al···G15 distance (r) in the corresponding transition state (**Al/G15-TS**) at the B3LYP-D3(BJ)/def2-TZVP level.

between G13′ and P in **G13′/P-Rea** is shorter than the separating distance between B(LA) and P(LB) in **B/P-Rea**. Surely, enough experimental evidence and theoretical calculation results are needed to comprehend the real reason behind it, but this is beyond the scope of this article.

Our DFT results given in Figure 3 indicate that the PC (**G13/P-PC**) for each **G13/P-Rea** case should exist because their calculated free-energy values are relatively lower than those of the corresponding reactants ranging from −20.3 to −5.3 kcal/mol. Moreover, our DFT evidence reveals that all five **G13/P-PC** structures have a similar three-center (O−G13−C) pattern, in which the oxygen atom of THF is attached to the G13 element of **G13/P-Rea**. Based on the available experimental report,[35] before THF is activated by the Al/P-FLP with the dimethylxanthene scaffold, the presence of a PC, in which the O element of THF is connected to the Al center of the Mes-substituted Al/P-FLP, is confirmed by the NMR evidence but without isolation (Scheme 2(a)). Nevertheless, the same intermediate produced by the reaction of THF and the C_6F_5-substituted Al/P-FLP, in which the O atom of THF is attached to the Al element of the latter, has not been experimentally detected (Scheme 2 [b]).[35]

The reaction barrier (kcal/mol) relative to the corresponding PC was found to increase as follows: **Al/P-TS** (29.6) < **Ga/P-TS** (30.4) < **In/P-TS** (34.6) < **Tl/P-TS** (38.8) < **B/P-TS** (47.6). Nevertheless, the order of ΔG_{RXN} (kcal/mol) follows a different trend from that of the reaction barrier: **Al/P-Prod** (−22.1) < **Ga/P-Prod** (−7.2) < **B/P-Prod** (−4.1) < **In/P-Prod** (3.5) < **Tl/P-Prod** (13.1). Notably, the free energy of **In/P-Prod** and **Tl/P-Prod** is higher than that of their corresponding starting materials, which strongly implies that THF ring-opening products of **In/P-Rea** and **Tl/P-Rea** are endothermic. Accordingly, on the basis of our theoretical conclusions, only intramolecular **Al/P-Rea** FLP bearing the dimethylxanthene scaffold can be energetically favorable to undergo the ring-opening reaction of THF. Indeed, according to one experimental report (Scheme 1(b)), the intramolecular C_6F_5-substituted P/Al-FLP based on the dimethylxanthene backbone can interact with THF to first generate the intermediate (**Al/P-PC**), which can be converted to yield the final ring-opening product (**Al/P-Prod**) after being heated to 80 °C.[35]

Furthermore, our computational evidence shown in Figure 3 reveals that the single-component **G13/P-Rea** FLP featuring a G13···P separation (Å) shows a distinct increasing trend: 2.655 (Al) < 2.731 (Ga) < 2.819 (In) < 3.001 (Tl) < 4.213 (B). This trend is similar to that of the activation barrier of the ring-opening reaction of THF by the corresponding **G13/P-Rea** FLP (Figure 3). Therefore, our theoretical finding indicates that the longer the separating distance between LA (G13) and LB (P) centers in the intramolecular **G13/P-Rea** FLP-type molecule bearing the dimethylxanthene scaffold, the higher the reaction barrier during its ring-opening reaction with THF.

Figure 4 exhibits relative energetic values of stationary points for the following mechanism: **Al/G15-Rea** + THF → **Al/G15-PC** → **Al/G15-TS** → **Al/G15-Prod**. The B3LYP results shown

https://doi.org/10.1021/acsomega.2c06194
ACS Omega 2023, 8, 5316−5331

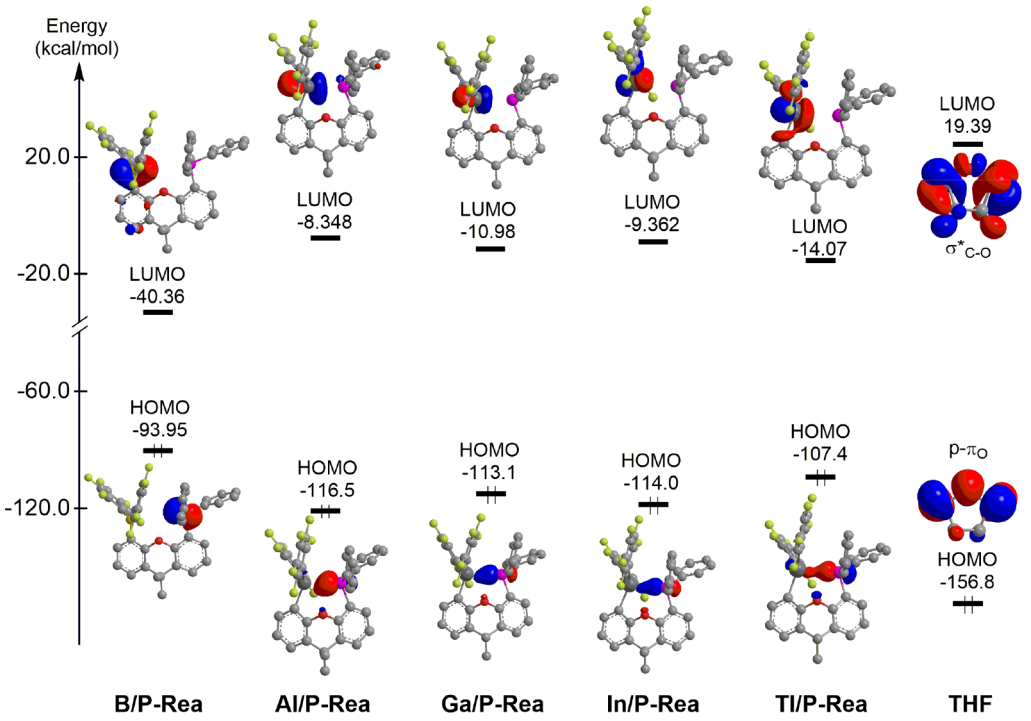

Figure 6. Frontier molecular orbitals (HOMOs and LUMOs) and calculated energy levels (in kcal/mol) for the dimethylxanthene scaffold **G13/P-Rea** FLP-type compounds and THF. Hydrogens are omitted for clarity.

Table 1. Calculated Energy Differences (in kcal/mol, B3LYP-D3(BJ)/def2-TZVP) of the HOMO and LUMO for G13/P-Rea FLPs and THF[a]

system	energy difference |FLP (HOMO) − THF (LUMO)|	energy difference |THF (HOMO) − FLP (LUMO)|
B/P-Rea + THF	113.3	116.5
Al/P-Rea + THF	136.9	148.5
Ga/P-Rea + THF	132.5	145.8
In/P-Rea + THF	133.4	147.4
Tl/P-Rea + THF	126.8	142.7

[a]Also see Figure 6.

in Figure 4 indicate that the energies of **Al/G15-PC** are lower than those of the corresponding reactants by approximately −28.7 to −20.3 kcal/mol. As mentioned in Scheme 2, only experimental evidence about the PC for the Al/P-FLP with the LA Al center attached to the Mes group has been reported.[35]

As shown in Figure 4, the separating Al···G15 distance (Å) of the reactant species (**Al/G15-Rea**) decreases in the following order: **Al/N-Rea** (4.913) > **Al/Bi-Rea** (3.544) > **Al/Sb-Rea** (2.934) > **Al/As-Rea** (2.787) > **Al/P-Rea** (2.655).[80] Moreover, our calculated free activation energy (kcal/mol), relative to its corresponding PC, for the ring-opening reaction of THF by **Al/G15-Rea** increases in the following order: 29.6 (P) < 33.8 (As) < 39.6 (Sb) < 47.7 (Bi) < 58.1 (N). Moreover, our theoretical computations collected in Figure 4 reveal that ΔG_{RXN} (kcal/mol) increases in the following order: **Al/P-Prod** (−22.1)[81] < **Al/As-Prod** (−10.2) < **Al/Sb-Prod** (0.7) < **Al/N-Prod** (11.0) < **Al/Bi-Prod** (12.5). Therefore, the aforementioned computational evidence indicates that only the dimethylxanthene-based **Al/P-Rea** FLP-assisted molecule is energetically feasible to undergo a ring-opening reaction with THF rather than the other four Al/G15-based FLPs. To our knowledge, only one available experimental work has reported that the Al/P-based FLP-type molecules, which are linked by a dimethylxanthene spacer, can cleave THF.[35]

Furthermore, a closer inspection of the optimized geometrical structure of **Al/G15-Rea** and the free activation barrier (ΔG_{ACT}) of its corresponding TS (**Al/G15-TS**) indicates that a good linear relationship ($\Delta G_{ACT} = 13.02r - 25.09$, correlation coefficient of 0.97) could be found when plotting the computed free activation barriers versus the separating Al···G15 distance (r) in **Al/G15-Rea** FLP (Figure 5).[82] Therefore, the C−O bond length must be stretched to gain the best orbital overlap between the Al···G15 centers of **Al/G15-Rea** FLP and the C···O elements of THF. Moreover, the separating Al···G15 distance in the dimethylxanthene scaffold Al/G15-based FLP-type molecule can be used as a reliable, quantitative measure of the barrier height for its ring-opening reaction with THF.

IV.2. FMO and EDA-NOCV. First, we explored the frontier molecular orbitals (FMOs)[83] of G13/P-containing FLP molecules featuring the dimethylxanthene scaffold and THF using the B3LYP-D3(BJ)/def2-TZVP level of theory, whose HOMO and LUMO along with the corresponding energetics were collected (Figure 6). Figure 6 reveals that the HOMO of **G13/P-Rea** is primarily located on the LB (P) site, whereas the LUMO of **G13/P-Rea** mostly resides on the LA (G13) site. We also calculated energy gaps between the FMOs of **G13/P-Rea** and THF, when both reactants react with each other to undergo the ring-opening reaction (eq 1). Table 1 shows the energy gap

https://doi.org/10.1021/acsomega.2c06194
ACS Omega 2023, 8, 5316−5331

Table 2. Results of EDA-NOCV at the ZORA-B3LYP-D3(BJ)/TZ2P//B3LYP-D3(BJ)/def2-TZVP Level of G13/P-TS[a]

	B/P-TS		Al/P-TS		Ga/P-TS		In/P-TS		Tl/P-TS	
fragments	B/P-Rea (S) + THF (S)	B/P-Rea (T) + THF (T)	Al/P-Rea (S) + THF (S)	Al/P-Rea (T) + THF (T)	Ga/P-Rea (S) + THF (S)	Ga/P-Rea (T) + THF (T)	In/P-Rea (S) + THF (S)	In/P-Rea (T) + THF (T)	Tl/P-Rea (S) + THF (S)	Tl/P-Rea (T) + THF (T)
ΔE_{INT}[b]	−66.6	−186.9	−67.8	−183.0	−61.8	−188.8	−62.1	−180.8	−60.4	−184.1
ΔE_{Pauli}	246.6	393.6	170.1	357.7	173.2	302.9	151.6	261.2	139.8	200.5
ΔE_{Elstat}[c]	−145.9 (46.6%)	−202.8 (34.9%)	−125.8 (52.9%)	−193.7 (35.8%)	−125.3 (53.3%)	−163.9 (33.3%)	−115.7 (54.2%)	−151.1 (34.2%)	−105.8 (52.8%)	−126.7 (32.9%)
ΔE_{Orb}[c]	−149.1 (47.6%)	−359.5 (61.9%)	−96.3 (40.5%)	−331.2 (61.3%)	−93.7 (39.9%)	−311.8 (63.4%)	−83.2 (38.9%)	−276.1 (62.5%)	−79.1 (39.5%)	−242.6 (63.1%)
$\Delta E_{Orb(1)}$[d]	−64.6 (43.3%)	−289.1 (80.4%)	−39.1 (40.6%)	−288.1 (87.0%)	−39.7 (42.4%)	−256.5 (82.3%)	−40.6 (48.9%)	−234.7 (85.0%)	−41.1 (51.9%)	−208.7 (86.0%)
$\Delta E_{Orb(2)}$[d]	−50.2 (33.6%)	−36.9 (10.3%)	−28.5 (29.6%)	−19.0 (5.7%)	−31.7 (33.8%)	−22.4 (7.2%)	−23.9 (28.7%)	−17.9 (6.5%)	−21.5 (27.2%)	−17.6 (7.2%)
ΔE_{Rest}[d]	−34.4 (23.0%)	−33.4 (9.3%)	−28.6 (29.8%)	−24.1 (7.3%)	−22.3 (23.8%)	−32.8 (10.5%)	−18.6 (22.4%)	−23.5 (8.5%)	−16.6 (20.9%)	−16.3 (6.7%)
ΔE_{Disper}[c]	−18.2 (5.8%)	−18.2 (3.1%)	−15.8 (6.6%)	−15.8 (2.9%)	−16.0 (6.8%)	−16.0 (3.3%)	−14.8 (6.9%)	−14.8 (3.3%)	−15.3 (7.7%)	−15.3 (4.0%)

[a]Fragments are **G13/P-Rea** and THF in singlet (S) and triplet (T) electronic states. All energy values are in kcal/mol. [b]$\Delta E_{INT} = \Delta E_{Elstat} + \Delta E_{Pauli} + \Delta E_{Orb} + \Delta E_{Disper}$. [c]The values in parentheses offer the percentage contribution to the total attractive interactions ($\Delta E_{Elstat} + \Delta E_{Orb} + \Delta E_{Disper}$). [d]The values in parentheses offer the percentage contribution to the total orbital interactions (ΔE_{ORB})

between the HOMO of **G13/P-Rea** and the LUMO of THF, which is smaller (113.3−136.9 kcal/mol) than that between the HOMO of THF and the LUMO of **G13/P-Rea** (116.5−148.5 kcal/mol). Consequently, our above theoretical observations indicate that the predominant interaction should take place between the HOMO of **G13/P-Rea** and the LUMO of THF. The EDA-NOCV results schematically shown below will again confirm the above FMO evidence.

The results of EDA-NOCV taking **G13/P-Rea** and THF as fragments are presented in Table 2 to gain more information of the bonding situations in **G13/P-TS**. As mentioned in Section III, two bonding interaction models (singlet−singlet interaction and triplet−triplet interaction) for the closed-shell and open-shell fragments, respectively, were utilized in this study. The results of EDA provided stronger FLP−THF interactions between triplet **G13/P-Rea** and triplet THF (ΔE_{INT} = −188.8 − −180.8 kcal/mol), whereas the weak bonding was calculated between the singlet fragment **G13/P-Rea** and singlet THF (ΔE_{INT} = −67.8 − −60.4 kcal/mol). Selecting the bonding model that could better represent the studied set of systems is challenging. However, previous studies have shown that a simple way to select the bonding model is to evaluate the ΔE_{Orb} value for each scheme.[84] In general, the bonding model that produces the smallest ΔE_{Orb} value can be used as an efficient indicator to describe the bonding situation because it requires the least alteration in the electronic charge distribution to generate the electronic structure of the system. Table 2 demonstrates that the fragments **G13/P-Rea** and THF for the singlet−singlet model have smaller ΔE_{Orb} values (−149.1 to −79.1 kcal/mol), whereas the corresponding fragments for the triplet−triplet model have higher ΔE_{Orb} values (−359.5 to −242.6 kcal/mol). Therefore, the former model is suitable for discussing the bonding situations between **G13/P-Rea** and THF.

More valuable information is obtained from the breakdown of the ΔE_{Orb} term into pairwise orbital contributions, which links the numerical results to the frontier orbital model (Figure 6). The EDA-NOCV results for **G13/P-TS** in the S−S model (Table 2) indicate that the strongest orbital interaction is dominated by $\Delta E_{Orb(1)}$, which may contribute to the total orbital interaction energy by 40.6−51.9%. However, the next smaller orbital interaction, namely, $\Delta E_{Orb(2)}$, contributes about 27.2−33.8% to ΔE_{Orb}. Consequently, they yield 70.2−79.1% of the total ΔE_{Orb}. The profile of deformation densities ($\Delta\rho_n$) associated with $\Delta E_{Orb(n)}$ is schematically represented in Figure 7, in which the direction of the charge flow is from the red to blue area in the color code. Figure 7 reveals that for the donor−acceptor interaction, $\Delta E_{Orb(1)}$ is the principal contributor of the orbital interaction, which corresponds to the transfer of electronic density from the lone pair of phosphorus to the empty σ^* orbital of THF, i.e., the lone pair (P) → the empty σ^*(C−O). On the contrary, $\Delta E_{Orb(2)}$ is the next contributor of the orbital interaction, which corresponds to the transfer of electronic density from the filled p−π orbital of oxygen to the vacant σ^* orbital on the G13 element, i.e., the empty σ^*(G13) ← filled p-π(O).

In understanding the relative reactivity for the ring-opening reaction of THF by Al/G15-based FLP-mediated molecules, we first investigated the FMOs of **Al/G15-Rea** and THF with the B3LYP-D3(BJ)/def2-TZVP method, whose calculated results are collected in Figure 8. Figure 8 revels that the HOMO of **Al/G15-Rea** primarily resides on the LB G15 element, whereas the LUMO of **Al/G15-Rea** is located on the LA aluminum element. Moreover, we calculated the energy gaps between the HOMO of

https://doi.org/10.1021/acsomega.2c06194
ACS Omega 2023, 8, 5316−5331

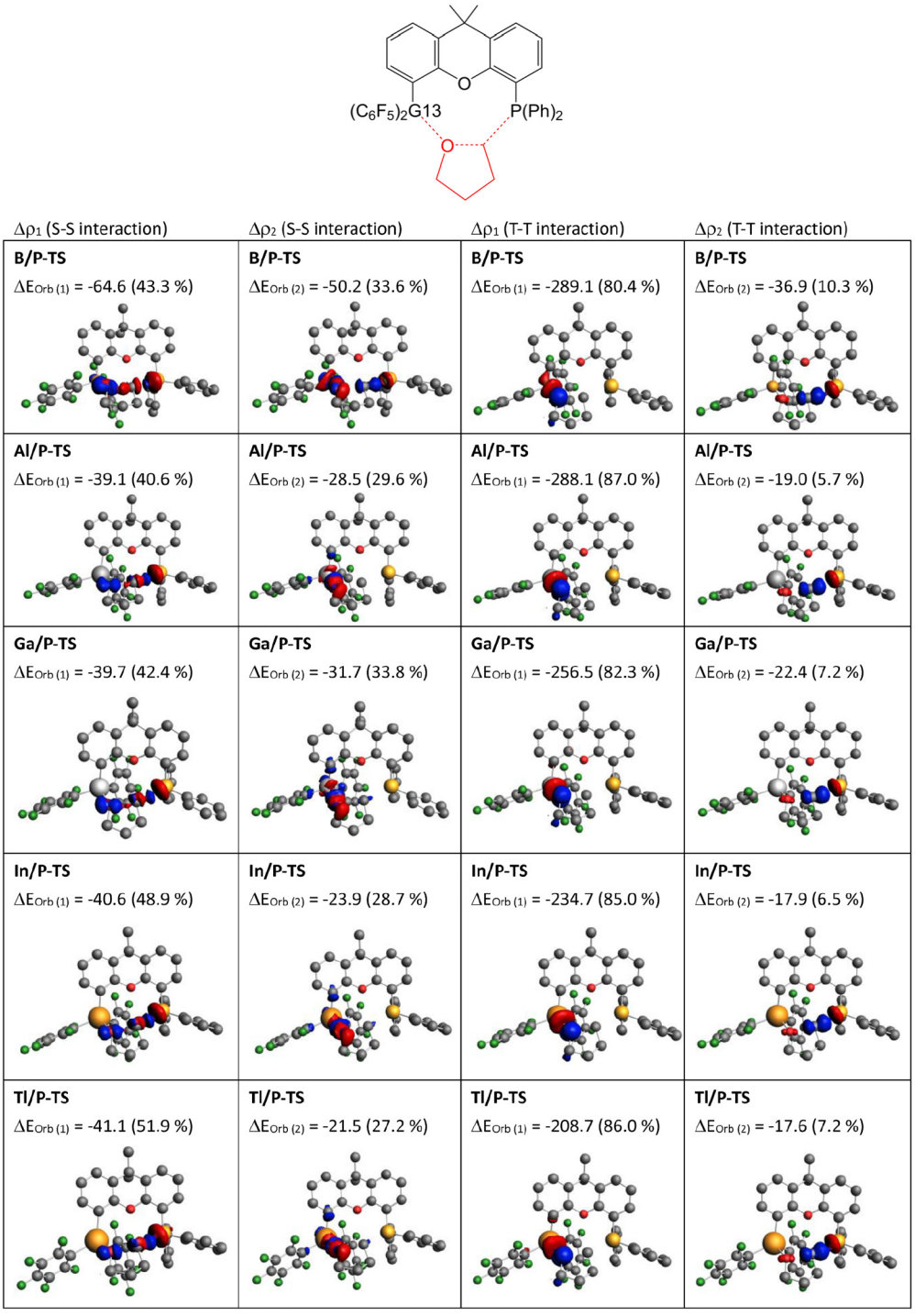

Figure 7. Plots of deformation densities, $\Delta\rho(r)$, of the pairwise orbital interactions in **G13/P-TS** at the ZORA-B3LYP-D3(BJ)/TZ2P//B3LYP-D3(BJ)/def2-TZVP level. Also see Table 2. Hydrogen atoms are omitted for clarity.

Al/G15-Rea and the LUMO of THF as well as those between the HOMO of THF and the LUMO of **Al/G15-Rea**, whose computational data are shown in Table 3. The latter data (136.6−153.9 kcal/mol) are obviously larger than the former data (108.1−137.6 kcal/mol; Table 3). Again, the EDA-NOCV diagram shown below will confirm the above FMO observations.

In uncovering the bonding nature of the interaction between the dimethylxanthene-linked Al/G15-FLP molecule and THF, we performed EDA-NOCV on their electronic structures to provide a strong basis for the mechanistic understanding. Similar to previous EDA-NOCV analyses for **G13/P-TS** cases shown in Table 2, the S−S and T−T models were applied to explore the bonding nature of the electronic structures of TSs (**Al/G15-TS**). As previously mentioned,[84] the size of the total orbital interactions (ΔE_{Orb}) can be used as an efficient indicator to justify the correct partitioning scheme because a low absolute ΔE_{Orb} value requires the least alteration in the electronic charge distribution to generate the electronic structure of the system. As shown in Table 4, 10 different fragmentation patterns, concerning the S−S and T−T models, are considered for all 5

https://doi.org/10.1021/acsomega.2c06194
ACS Omega 2023, 8, 5316−5331

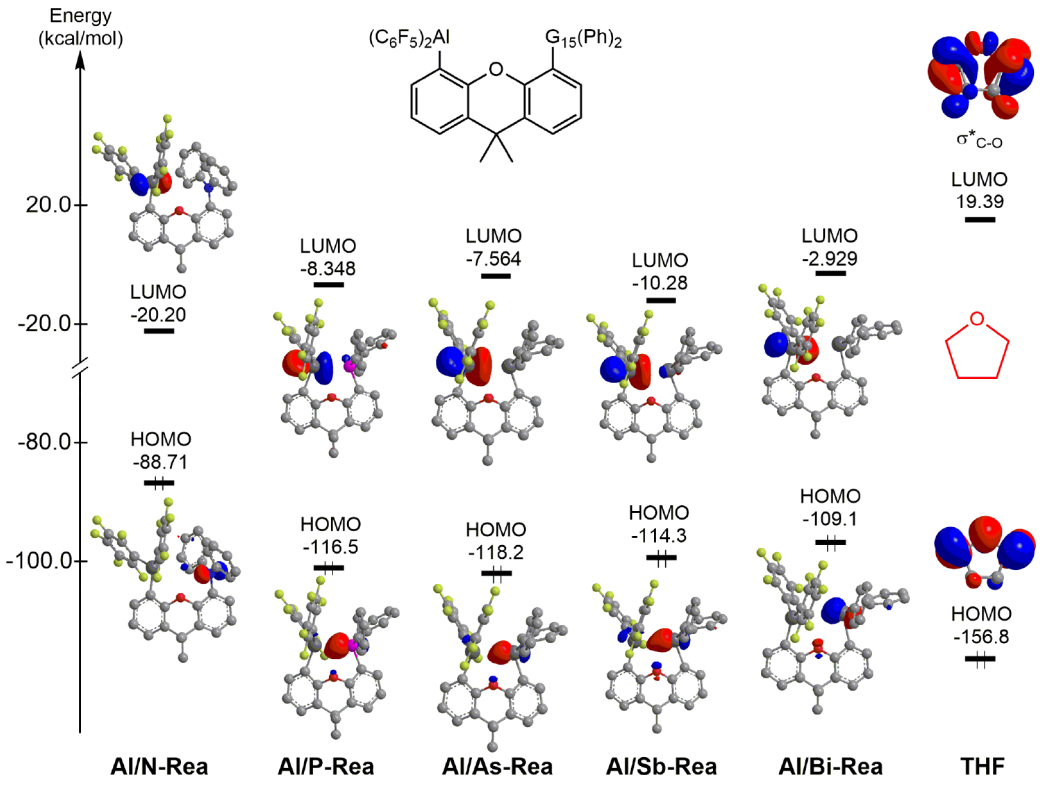

Figure 8. Frontier molecular orbitals (HOMOs and LUMOs) and calculated energy levels (in kcal/mol) for the dimethylxanthene scaffold **Al/G15-Rea** FLPs and THF. Hydrogens are omitted for clarity.

Table 3. Calculated Energy Differences (in kcal/mol, B3LYP-D3(BJ)/def2-TZVP) of the HOMOs and LUMOs for Al/G15-Rea FLPs and THF[a]

system	energy difference |FLP (HOMO) − THF (LUMO)|	energy difference |THF (HOMO) − FLP (LUMO)|
Al/N-Rea + THF	108.1	136.6
Al/P-Rea + THF	135.9	148.5
Al/As-Rea + THF	137.6	149.2
Al/Sb-Rea + THF	133.7	146.5
Al/Bi-Rea + THF	128.4	153.9

[a]Also see Figure 8.

calculated TSs, **Al/G15-TS**. Examining the strength of orbital interactions (Table 5), the S−S interaction provides lower **Al/G15-TS** values for ΔE_{Orb} than the T−T interaction. For example, Table 4 demonstrates that the ΔE_{Orb} values of all **Al/G15-TS** for the S−S interaction range from −119.9 to −96.3 kcal/mol, while those for the T−T model range from −331.2 to −298.4 kcal/mol. Consequently, the data in Table 4 indicate that the best representation of the bonding situation in all five **Al/G15-TS** is obtained by the S−S interaction. Notably, this theoretical finding is consistent with that of the previous five **G13/P-TS** systems shown in Table 2.

Using the NOCV[61−64] method, the crucial information can be obtained from the further decomposition of ΔE_{Orb} into pairwise orbital interaction, $\Delta E_{Orb(n)}$. As shown in Table 4, in five **Al/G15-TS**s utilizing the S−S interaction, only two dominant contributions ($\Delta E_{Orb(1)}$ and $\Delta E_{Orb(2)}$) are obtained, which provide at least 70% to ΔE_{Orb}. In addition, one intriguing feature for NOCV analyses is that the charge migration associated with pairwise orbital interactions can be schematically represented as deformation densities $\Delta\rho$. Consequently, $\Delta E_{Orb(1)}$ and $\Delta E_{Orb(2)}$ can be identified using the associated deformation densities ($\Delta\rho_1$ and $\Delta\rho_2$, respectively) and the connected occupied and vacant fragment orbitals (Figure 9). Notably, the color code indicates that the charge flow is red → blue. Figure 9 shows that the strongest orbital contribution in **Al/G15-TS** is obtained from the donation of the HOMO of **Al/G15-Rea** (i.e., the LP of LB G15 center) to the LUMO of THF (i.e., the vacant C−O σ^* orbital), with $\Delta E_{Orb(1)}$ ranging from −54.3 to −39.1 kcal/mol. Moreover, the second strongest orbital interaction $\Delta E_{Orb(2)}$ = −34.1 − −28.5 kcal/mol is obtained from the donation of the HOMO of THF (i.e., the filled p−π orbital on O) to the LUMO of **Al/G15-Rea** (i.e., the vacant σ^* orbital on LA Al center). In other words, the EDA-NOCV result indicates that the FLP-to-THF forward bonding (i.e., $\Delta E_{Orb(1)}$) plays a significant role in determining the contribution of the orbital interaction to the bonding conditions between **Al/G15-Rea** and THF, while the THE-to-FLP back bonding (i.e., $\Delta E_{Orb(2)}$) plays a minor role in such bonding interactions. From the theoretical analyses for both **G13/P-TS** and **Al/G15-TS** cases, it is therefore known that the theoretical information based on EDA-NOCV can be used to comprehensively understand the bonding situations in the ring-opening reaction of THF by the dimethylxanthene backbone Al/G15-based FLP-related molecules.

https://doi.org/10.1021/acsomega.2c06194
ACS Omega 2023, 8, 5316−5331

Table 4. Results of EDA-NOCV at the ZORA-B3LYP-D3(BJ)/TZ2P//B3LYP-D3(BJ)/def2-TZVP Level of G13/P-TS[a]

	Al/N-TS		Al/P-TS		Al/As-TS		Al/Sb-TS		Al/Bi-TS	
fragments	Al/N-Rea (S) + THF (S)	Al/N-Rea (S) + THF (S)	Al/P-Rea (S) + THF (S)	Al/P-Rea (T) + THF (T)	Al/As-Rea (S) + THF (S)	Al/As-Rea (T) + THF (T)	Al/Sb-Rea (S) + THF (S)	Al/Sb-Rea (T) + THF (T)	Al/Bi-Rea (S) + THF (S)	Al/Bi-Rea (T) + THF (T)
ΔE_{INT}[b]	−65.7	−162.3	−67.8	−183.0	−69.6	−195.4	−71.1	−184.8	−77.3	−172.2
ΔE_{Pauli}	193.3	333.8	170.1	357.7	174.1	341.3	181.5	347.4	195.9	367.6
ΔE_{Elstat}[c]	−126.5(48.9%)	−179.5(36.2%)	−125.8(52.9%)	−193.7(35.8%)	−128.1(52.6%)	−194.4(36.2%)	−132.7(52.5%)	−199.2(37.4%)	−140.5(51.4%)	−210.0(38.9%)
ΔE_{Orb}[c]	−114.2 (−114.2%)	−298.4 (−298.4%)	−96.3(40.5%)	−331.2(61.3%)	−100.8(−100.8%)	−327.6(−327.6%)	−106.7(−106.7%)	−319.7(−319.7%)	−119.9 (−119.9%)	−316.9(−316.9%)
$\Delta E_{Orb(1)}$[d]	−47.4(41.5%)	−256.5(86.0%)	−39.1(40.6%)	−288.1(87.0%)	−41.7(41.4%)	−282.2(86.1%)	−45.7(42.8%)	−272.0(85.1%)	−54.3(45.3%)	−263.6(83.2%)
$\Delta E_{Orb(2)}$[d]	−34.1(29.9%)	−17.3(5.8%)	−28.5(29.6%)	−19.0(5.7%)	−29.6(29.4%)	−20.2(6.2%)	−30.7(28.8%)	−21.3(6.7%)	−32.6(27.2%)	−24.3(7.7%)
ΔE_{Rest}[d]	−32.7(28.6%)	−24.6(8.2%)	−28.6(29.8%)	−24.1(7.3%)	−29.5(29.3%)	−25.2(7.7%)	−30.2(28.3%)	−26.3(8.2%)	−33.0(27.5%)	−29.0(9.2%)
ΔE_{Disper}[c]	−18.3(7.0%)	−18.3(3.7%)	−15.8(6.6%)	−15.8(2.9%)	−14.8(6.1%)	−14.8(2.8%)	−13.2(5.2%)	−13.2(2.5%)	−12.8(4.7%)	−12.8(2.4%)

[a]Fragments are **Al/G15-Rea** and THF in singlet (S) and triplet (T) electronic states. All energy values are in kcal/mol. [b]$\Delta E_{INT} = \Delta E_{Elstat} + \Delta E_{Pauli} + \Delta E_{Orb} + \Delta E_{Disper}$. [c]The values in parentheses offer the percentage contribution to the total attractive interactions ($\Delta E_{Elstat} + \Delta E_{Orb} + \Delta E_{Disper}$). [d]The values in parentheses offer the percentage contribution to the total orbital interactions (ΔE_{Orb}).

Table 5. Energy Decomposition Analysis for the Ring-Opening Reaction of THF by Dimethylxanthene Backbone G13/P-TS[a,b]

entry	B/P-TS	Al/P-TS	Ga/P-TS	In/P-TS	Tl/P-TS
ΔE_{ACT}[b,c]	13.9	−3.9	14.6	17.8	25.0
$\Delta E_{DEF,THF}$	46.7	28.8	38.9	40.9	44.1
$\Delta E_{DEF,G13/P-Rea}$	34.8	35.1	37.5	39.0	41.3
ΔE_{INT}	−66.6	−67.8	−61.8	−62.1	−60.4

[a]At the ZORA-B3LYP-D3(BJ)/TZ2P//B3LYP-D3(BJ)/def2-TZVP level. [b]All in kcal mol^{-1}. [c]$\Delta E_{ACT} = \Delta E_{DEF,THF} + \Delta E_{DEF,G13/P-Rea} + \Delta E_{INT}$.

IV.3. Origin of Activation Energies Investigated by ASM. In obtaining more information about the origin of activation barriers for the ring-opening reactions of THF by the **G13/P-Rea** FLP-associated molecule, ASM has been utilized in the present work. Notably, the ASM involves the decomposition of the electronic reaction barrier (ΔE_{ACT}) into the deformation energy ($\Delta E_{DEF,THF}$ and $\Delta E_{DEF,G13/P-Rea}$; Scheme 3), which is associated with the rigidity of the reactants and the interaction energy (ΔE_{INT}) among deformed fragments, whose calculated results are presented in Table 5 and Figure 10. Figure 10 shows that the deformation energy of THF ($\Delta E_{DEF,THF}$) is a decisive factor in determining the reactivity trend in such ring-opening reactions of THF by **G13/P-Rea** FLPs. This phenomenon can be understood when **G13/P-Rea** and THF approach each other. In obtaining good orbital overlaps between the carbon element of THF and the phosphorus element of **G13/P-Rea** and between the oxygen element of THF and the G13 element of **G13/P-Rea**, the C−O bond of THF must stretch to match the separating distance between G13 and P in **G13/P-Rea**. As shown in Scheme 3, the cleavage of the C−O bond in THF accompanies the formation of C−P and O−G13 chemical bonds. Our B3LYP results shown in Figure 3 demonstrate that **G13/P-Rea** has the longest separating B(LA)···P(LB) distance in the **G13/P-Rea** FLPs. Thus, the C−O bond in THF is elongated to perform effective orbital overlaps with the **B/P-Rea** FLP. Consequently, $\Delta E_{DEF,\ THF}$ of **B/P-TS** becomes the largest (Table 5 and Figure 10). This phenomenon leads to the highest activation barrier for **B/P-TS** when **B/P-Rea** undergoes the ring-opening reaction with THF.

Furthermore, our B3LYP computational results shown in Figure 3 indicate that there was an increasing trend in the calculated C−O bond of **G13/P-TS**: **Al/P-TS** (35.1%) < **B/P-TS** (35.4%) < **Ga/P-TS** (36.5%) < **In/P-TS** (38.1%) < **Tl/P-TS** (39.8%). This result is relative to that in the initial THF (1.431 Å). Notably, the trend for the elongated C−O bond length in the geometry of **G13/P-TS** indicates its corresponding barrier height. Our DFT results shown in Figure 3 and Table 5 demonstrate that the reaction barrier (kcal/mol) increases as follows: **Al/P-TS** (−3.9) < **B/P-TS** (13.9) < **Ga/P-TS** (14.6) < **In/P-TS** (17.8) < **Tl/P-TS** (35.0). The aforementioned theoretical evidence is consistent with the Hammond postulate,[85] which indicates that an early TS would be accompanied by a smaller barrier height. Accordingly, our theoretical evidence suggests that the key factor affecting the activation energy of **G13/P-TS** is highly dependent on the structural deformation energy of THF during its ring-opening reaction.

Again, the detailed ASM analyses of two representative cases (i.e., **B/P-TS** and **Al/P-TS**) were performed along the reaction profile to elucidate the different reactivity of **G13/P-Rea** toward

https://doi.org/10.1021/acsomega.2c06194
ACS Omega 2023, 8, 5316−5331

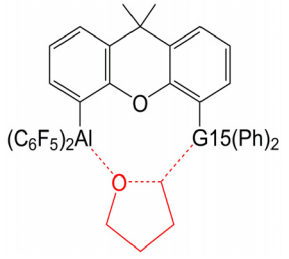

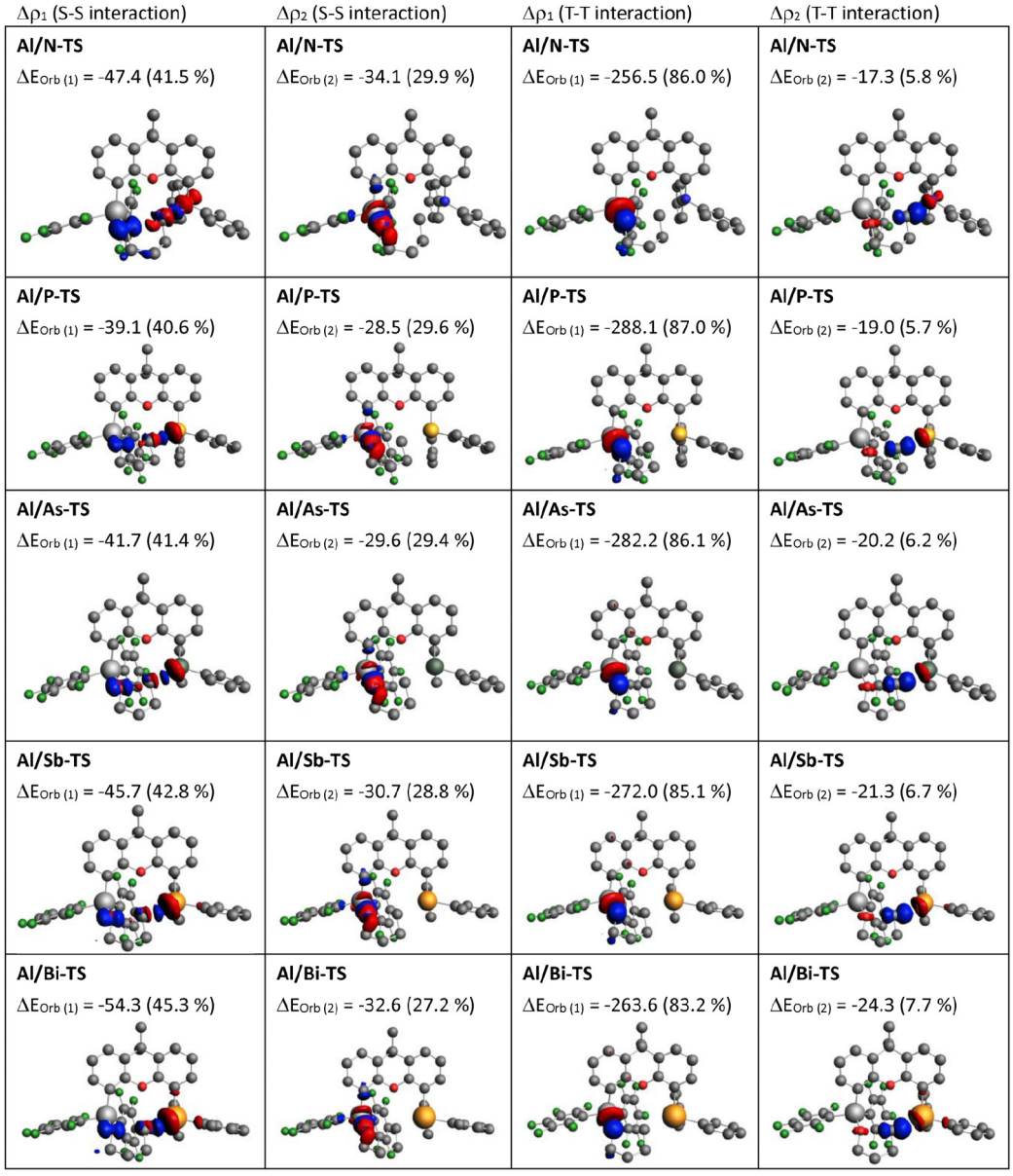

Figure 9. Plots of deformation densities, $\Delta\rho(r)$, of the pairwise orbital interactions in **Al/G15-TS** at the ZORA-B3LYP-D3(BJ)/TZ2P//B3LYP-D3(BJ)/def2-TZVP level. Also see Table 4. Hydrogen atoms are omitted for clarity.

the ring-opening reaction of THF.[86] The ASM results shown in Figure 11 reveal that a smaller ΔE_{ACT} for **Al/P-TS** can be attributed to the low deformation energy of the THF fragment ($\Delta E_{DEF,THF}$). This finding is consistent with previous examinations shown in Table 5 and Figure 10. For example, Figure 11 shows that the $\Delta E_{DEF,G13/P\text{-}Rea}$ value (kcal/mol) of **B/P-TS** and **Al/P-TS** was 33.1 and 30.5 at the C−O distance of 1.822 Å, whereas the interaction energy (kcal/mol) of **B/P-TS** and **Al/P-TS** was −45.9 and −49.9, respectively. The two aforementioned energy parameters are similar to each other; therefore, $\Delta E_{DEF,G13/P\text{-}Rea}$ and ΔE_{INT} cannot influence the barrier height. The $\Delta E_{DEF,THF}$ (kcal/mol) value for **Al/P-TS** (14.8) and **B/P-TS** (25.6) can affect their respective activation energies, that is, **Al/P-TS** (−4.6) and **B/P-TS** (12.8).

We again applied the ASM approach to the ring-opening reaction of THF involving the Al/G15-based FLP-associated

https://doi.org/10.1021/acsomega.2c06194
ACS Omega 2023, 8, 5316−5331

Scheme 3. Schematic Representation of the Ring-Opening Reaction of Dimethylxanthene Backbone G13/P-Rea with THF

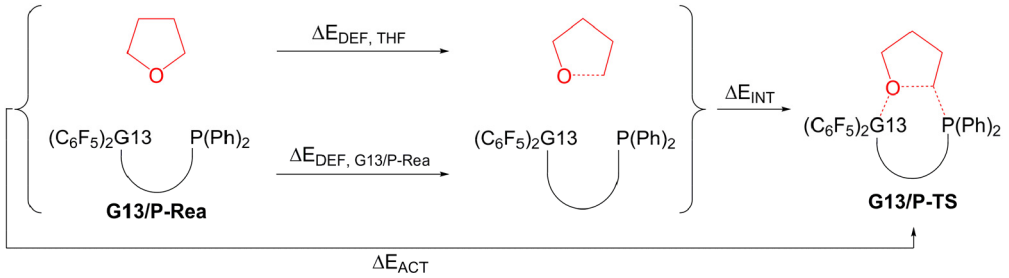

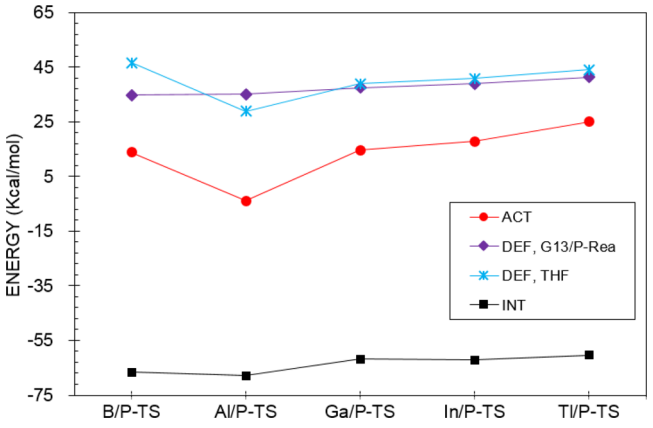

Figure 10. Plot of energy decomposition analysis of ΔE_{ACT} for the ring-opening reactions of **G13/P-Rea** with THF. Values are taken from Table 5.

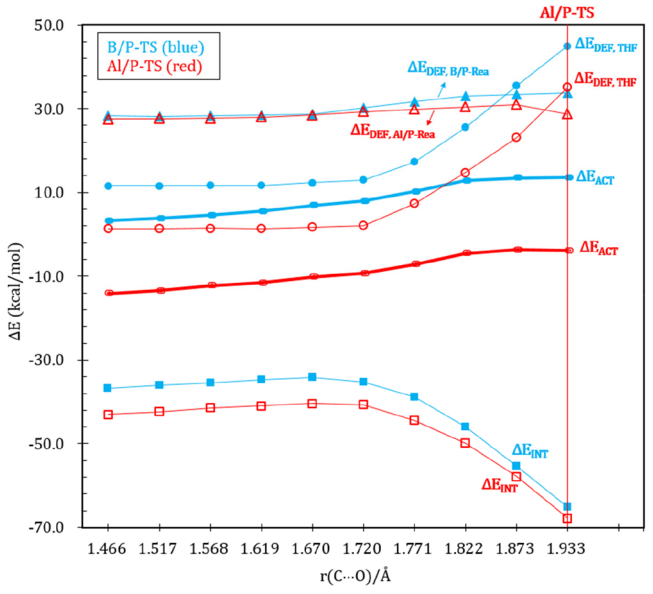

Figure 11. Comparative activation strain diagrams for the ring-opening reactions of THF involving dimethylxanthene backbone **B/P-TS** (blue lines) and **Al/P-TS** (red lines) along the reaction coordinate projected onto the C···O bond distance, calculated at the ZORA-B3LYP-D3(BJ)/TZ2P//B3LYP-D3(BJ)/def2-TZVP level.

molecules bearing the dimethylxanthene scaffold to understand the reactivity trend (Scheme 4, Table 6, and Figure 12). Similar to the **G13/P-TS** cases discussed earlier, the activation energy (ΔE_{ACT}) can be composed of two deformation energies ($\Delta E_{DEF,\ THF}$ + $\Delta E_{DEF,Al/G15\text{-}Rea}$) and the interaction energy (ΔE_{INT}). As shown in Figure 12, the deformation energy of THF could be a decisive factor in influencing the barrier heights for such ring-opening reactions. As shown in Figure 9, the separating Al(LA)···N(LB) distance in the **Al/N-Rea** FLP species is the largest (4.193 Å). In obtaining a better orbital overlap between THF and the **Al/N-Rea** FLP, a C−O bond of THF must be elongated, and the deformation energy of THF ($\Delta E_{DEF,THF}$) must be increased. This technique, in turn, leads to the highest reaction barrier for the ring-opening reaction of THF by the **Al/N-Rea** FLP with a dimethylxanthene scaffold (Figure 4). Moreover, based on the calculated geometrical structure of **Al/G15-TS** shown in Figure 4, the broken C−O bond length of the THF fragment increases as **Al/P-TS** (35.1%) < **Al/As-TS** (39.9%) < **Al/Sb-TS** (45.7%) < **Al/Bi-TS** (56.1%) < **Al/N-TS** (74.4%), which is relative to that of the original THF (1.431 Å). This structural trend is consistent with the trend of free reaction barriers for **Al/G15-TS** as discussed earlier. Therefore, the aforementioned theoretical finding is consistent with the Hammond postulate,[85] which indicates that "the more reactant-like the TS, the smaller its activation barrier".

Two representative systems, **Al/N-TS** and **Al/P-TS**, have been selected for theoretical analysis by using a detailed ASM approach, whose calculated results are collected in Figure 13.[86] Our B3LYP investigations clearly reveal that only the deformation energy of THF ($\Delta E_{DEF,THF}$) plays a significant role in influencing barrier heights of the ring-opening reactions of THF by the Al/G15-based FLP-type molecules featuring a dimethylxanthene backbone. For example, Figure 13 indicates that at a C−O distance of 1.822 Å the $\Delta E_{DEF,G13/P\text{-}Rea}$ (kcal/mol) values of **Al/N-TS** and **Al/P-TS** are approximately 10.3 and 30.5, whereas the interaction energies (kcal/mol) of **Al/N-TS** and **Al/P-TS** are −30.6 and −49.9, respectively. The sums of the two aforementioned energy parameters ($\Delta E_{DEF,G13/P\text{-}Rea}$ + ΔE_{INT}) are similar to each other. Consequently, $\Delta E_{DEF,G13/P\text{-}Rea}$ and ΔE_{INT} cannot effectively control the reaction barrier. Only the $\Delta E_{DEF,THF}$ (kcal/mol) values for **B/P-TS** (24.3) and **Al/P-TS** (14.8) can affect their respective activation energies, that is, **B/P-TS** (4.1) and **Al/P-TS** (−4.6). Accordingly, the above theoretical observation is in good agreement with the findings shown in Table 6 and Figure 12.

V. CONCLUSIONS

The present study reports on the theoretical investigations of the chemistry of the THF ring-opening reaction by intramolecular G13/G15-FLPs based on the dimethylxanthene scaffold. Several theoretically sophisticated methods, including the FMO theory, ASM, and the EDA−NOCV approach, have been utilized in this work to gain insights into the origin of activation barriers and reactivity trends. Several crucial conclusions can be drawn as follows:

https://doi.org/10.1021/acsomega.2c06194
ACS Omega 2023, 8, 5316−5331

Scheme 4. Schematic Representation of the Ring-Opening Reaction of Dimethylxanthene Backbone Al/G15-Rea with THF

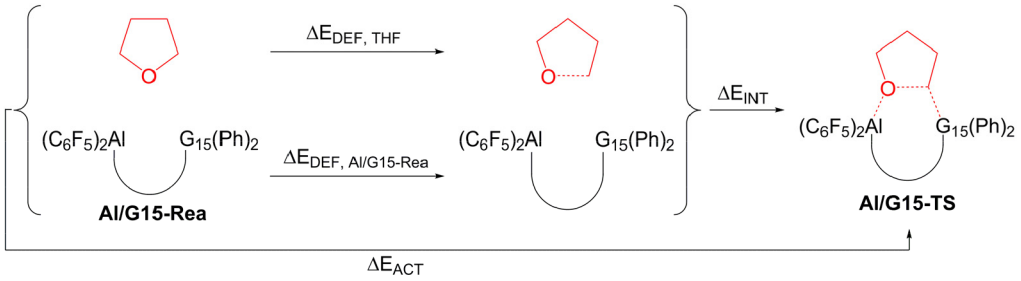

Table 6. Energy Decomposition Analysis of the Ring-Opening Reaction of THF by Dimethylxanthene Backbone Al/G15-Rea

entry	Al/N-TS	Al/P-TS	Al/As-TS	Al/Sb-TS	Al/Bi-TS
ΔE_{ACT} [a,b,c]	14.9	−3.9	−1.7	−0.2	1.2
$\Delta E_{DEF,THF}$	54.4	28.8	40.7	47.0	57.6
$\Delta E_{DEF,Al/G15-Rea}$	26.2	35.1	27.3	23.8	20.9
ΔE_{INT}	−65.7	−67.8	−69.6	−71.1	−77.3

[a]At the ZORA-B3LYP-D3(BJ)/TZ2P//B3LYP-D3(BJ)/def2-TZVP level. [b]All in kcal mol^{-1}. [c]$\Delta E_{ACT} = \Delta E_{DEF,THF} + \Delta E_{DEF, Al/G15-Rea} + \Delta E_{INT}$.

(1) Our theoretical examinations predict that in the intramolecular dimethylxanthene-linked **G13/P-Rea** FLP-assisted molecules, only **Al/P-Rea** FLP evidently is energetically favorable to undergo the ring-opening reaction of THF.

(2) Our calculated evidence indicates that in Al-based and G15-based **Al/G15-Rea** FLP-related compounds featuring the dimethylxanthene scaffold, only **Al/P-Rea** FLP can be energetically feasible to cleave THF without difficulty.

(3) By comparing all ring-opening reactions of THF studied in this work, our B3LYP analyses demonstrate that the dimethylxanthene backbone **Al/G15-Rea** FLPs can undergo the ring-opening reaction of THF more easily than the congener **G13/P-Rea** FLPs since the former has a lower reaction barrier and a larger exergonicity than the latter.

(4) Our EDA analyses indicate that the donor−acceptor model rather than the electron-sharing model controls the bonding natures of their TSs. Furthermore, it is known with some certainty that both forward and backward donations, which are widely used to explain bonding scenarios in organometallic chemistry, will be important. In the past computational studies, this is a quantity that could be difficult to pin down. This work is the first theoretical study to prove quantitatively that the two donations contribute differently to chemical bonding. Our theoretical findings quantitatively demonstrate that the forward donation is the FLP-to-THF interaction (a LP(G15) → σ^*(C−O)), which predominantly governs such ring-opening reactions of THF by the dimethylxanthene backbone G13/G15-based FLPs. On the other hand, the back-bonding component is the THF-to-FLP interaction (an empty σ^*(G13) ← filled p−π(O)), which plays a minor role in such bonding situations.

(5) It is already known that the size of THF is smaller than that of the dimethylxanthene-based G13/G15-based FLP. Our ASM study clearly indicates that when G13/G15-FLP and THF are close enough to each other to react, the C−O bond of THF must be elongated to effectively overlap with G13/G15-FLP. As a result, the longer the C−O bond is stretched, the more the structural deformation energy of THF will be increased. Namely, when they form a transition state, the geometric structure of THF would be greatly deformed, resulting in its deformation energy being larger. This, in turn, becomes the key factor in determining the whole activation energy.

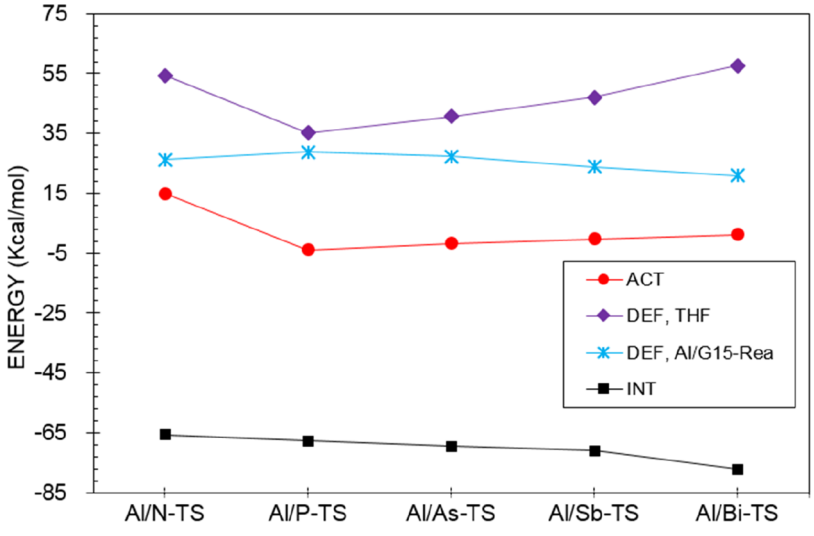

Figure 12. Plot of energy decomposition analysis of ΔE_{ACT} for the ring-opening reactions of **Al/G15-Rea** with THF. Values are taken from Table 6.

https://doi.org/10.1021/acsomega.2c06194
ACS Omega 2023, 8, 5316−5331

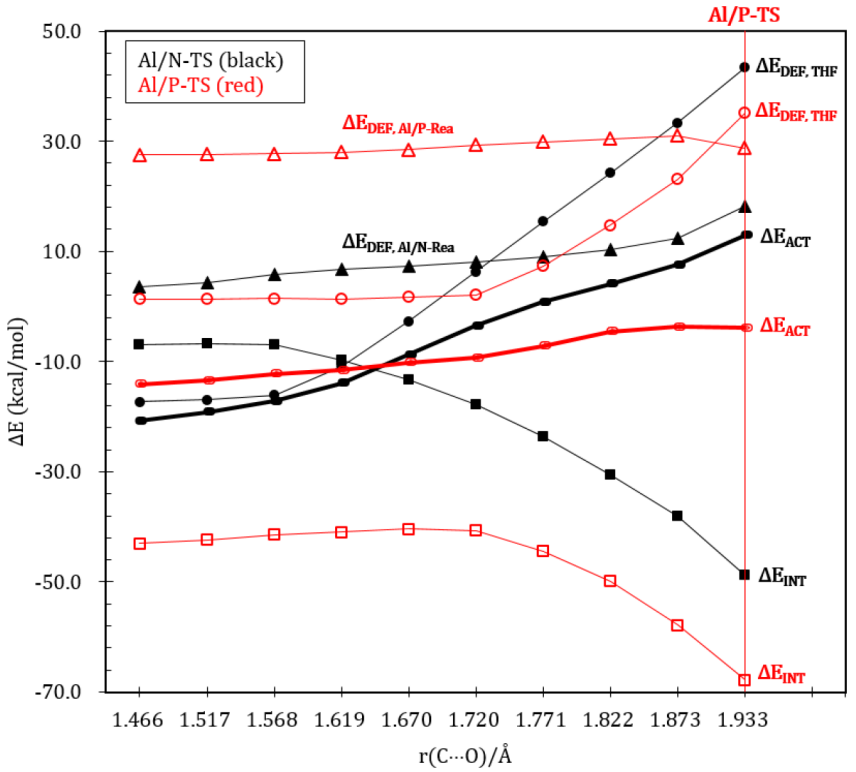

Figure 13. Comparative activation strain diagrams for the ring-opening reactions of THF involving the dimethylxanthene backbone **Al/N-TS** (black lines) and **Al/P-TS** (red lines) along the reaction coordinate projected onto the C···O bond distance, calculated at the ZORA-B3LYP-D3(BJ)/TZ2P//B3LYP-D3(BJ)/def2-TZVP level.

Accordingly, our B3LYP findings reveal that in the ring-opening reaction of THF by **G13/P-Rea** and **Al/G15-Rea** FLPs bearing the dimethylxanthene scaffold, the separating LA···LB distance in such FLP-type reactant species can be taken as a diagnostic tool to estimate the relative activation barriers.

(6) Our DFT results shown in this work indicate that the ring-opening reaction of THF by the **G13/G15-Rea** FLPs is consistent with Hammond's postulate. That is, the earlier the TS of the chemical reaction arrives, the smaller the activation energy.

■ ASSOCIATED CONTENT

Supporting Information

The Supporting Information is available free of charge at https://pubs.acs.org/doi/10.1021/acsomega.2c06194.

Sums of electronic and thermal free energies (PDF)

■ AUTHOR INFORMATION

Corresponding Author

Ming-Der Su − *Department of Applied Chemistry, National Chiayi University, Chiayi 60004, Taiwan; Department of Medicinal and Applied Chemistry, Kaohsiung Medical University, Kaohsiung 80708, Taiwan;* orcid.org/0000-0002-5847-4271; Email: midesu@mail.ncyu.edu.tw

Author

Zheng-Feng Zhang − *Department of Applied Chemistry, National Chiayi University, Chiayi 60004, Taiwan*

Complete contact information is available at: https://pubs.acs.org/10.1021/acsomega.2c06194

Author Contributions

Z.-F.Z. conducted all of the theoretical computations and analyzed the results. M.-D.S. supervised the research activities and contributed to the manuscript preparation. Both authors regularly discussed the progress of the research, reviewed the manuscript, and gave approval for the final version.

Notes

The authors declare no competing financial interest.

■ ACKNOWLEDGMENTS

The authors thank the National Center for High-Performance Computing of Taiwan. The National Science and Technology Council of Taiwan financially supported this research. Special thanks are also due to reviewers 1, 2, and 3 for very helpful suggestions and comments.

■ REFERENCES

(1) Welch, C. C.; Juan, R. R. S.; Masuda, J. D.; Stephan, D. W. Reversible, Metal-Free Hydrogen Activation. *Science* **2006**, *314*, 1124−1126.

(2) McCahill, J. S. J.; Welch, G. C.; Stephan, D. W. Reactivity of "frustrated Lewis pairs": three-component reactions of phosphines, a borane, and olefins. *Angew. Chem., Int. Ed.* **2007**, *46*, 4968−4971.

(3) Chase, P. A.; Welch, G. C.; Jurca, T.; Stephan, D. W. Metal-free catalytic hydrogenation. *Angew. Chem., Int. Ed.* **2007**, *46*, 8050−8053.

(4) Chase, P. A.; Jurca, T.; Stephan, D. W. Lewis acid-catalyzed hydrogenation: $B(C_6F_5)_3$-mediated reduction of imines and nitriles with H_2. *Chem. Commun.* **2008**, 1701−1703.

(5) Stephan, D. W. Frustrated Lewis pairs": a concept for new reactivity and catalysis. *Org. Biomol. Chem.* **2008**, *6*, 1535−1539.

(6) Stephan, D. W. Frustrated Lewis pairs: a new strategy to small molecule activation and hydrogenation catalysis. *Dalton Trans.* **2009**, *38*, 3129−3136.

(7) Mömming, C. M.; Otten, E.; Kehr, G.; Fröhlich, R.; Grimme, S.; Stephan, D. W.; Erker, G. Reversible Metal-Free Carbon Dioxide Binding by Frustrated Lewis Pairs. *Angew. Chem., Int. Ed.* **2009**, *48*, 6643−6646.
(8) Stephan, D. W.; Erker, G. Frustrated Lewis Pairs: Metal-free Hydrogen Activation and More. *Angew. Chem., Int. Ed.* **2010**, *49*, 46−76.
(9) Stephan, D. W.; Erker, G. Frustrated Lewis pair chemistry of carbon, nitrogen and sulfur oxides. *Chem. Sci.* **2014**, *5*, 2625−2641.
(10) Stephan, D. W. Frustrated Lewis Pairs: From Concept to Catalysis. *Acc. Chem. Res.* **2015**, *48*, 306−316.
(11) Stephan, D. W.; Erker, G. Frustrated Lewis Pairs: Development and Perspective. *Angew. Chem., Int. Ed.* **2015**, *54*, 6400−6441.
(12) Stephan, D. W.; Erker, G. Frustrated Lewis Pair Chemistry: Development and Perspectives. *Angew. Chem., Int. Ed.* **2015**, *54*, 6400−6441.
(13) Stephan, D. W. Frustrated Lewis Pairs. *J. Am. Chem. Soc.* **2015**, *137*, 10018−10032.
(14) Weicker, S. A.; Stephan, D. W. Main Group Lewis Acids in Frustrated Lewis Pair Chemistry: Beyond Electrophilic Boranes. *Bull. Chem. Soc. Jpn.* **2015**, *88*, 1003−1016.
(15) Stephan, D. W. The broadening reach of frustrated Lewis pair chemistry. *Science* **2016**, *354*, aaf7229-1−aaf7229-8.
(16) Kehr, G.; Erker, G. Frustrated Lewis Pair Chemistry: Searching for New Reactions. *Chem. Rec.* **2017**, *17*, 803−815.
(17) Scott, D. J.; Fuchter, M. J.; Ashley, A. E. Designing Effective 'Frustrated Lewis Pair' Hydrogenation Catalysts. *Chem. Soc. Rev.* **2017**, *46*, 5689−5700.
(18) Jupp, A. R.; Stephan, D. W. New Directions for Frustrated Lewis Pair Chemistry. *Trends in Chemistry* **2019**, *1*, 35−48.
(19) Sadek, O.; Bouhadir, G.; Bourissou, D. Lewis pairing and frustration of group 13/15 elements geometrically enforced by (ace) naphthalene, biphenylene and (thio) xanthene backbones. *Chem. Soc. Rev.* **2021**, *50*, 5777−5805.
(20) Chernichenko, K.; Lindqvist, M.; Kótai, B.; Nieger, M.; Sorochkina, K.; Pápai, I.; Repo, T. Metal-Free sp2-C-H Borylation as a Common Reactivity Pattern of Frustrated 2-Aminophenylboranes. *J. Am. Chem. Soc.* **2016**, *138*, 4860−4868.
(21) Chen, G.-Q.; Kehr, G.; Mück-Lichtenfeld, C.; Daniliuc, C. G.; Erker, G. Phospha-Claisen Type Reactions at Frustrated Lewis Pair Frameworks. *J. Am. Chem. Soc.* **2016**, *138*, 8554−8559.
(22) Liu, K. L.; Lalancette, R. A.; Jakle, F. B-N Lewis Pair Functionalization of Anthracene: Structural Dynamics, Optoelectronic Properties, and O_2 Sensitization. *J. Am. Chem. Soc.* **2017**, *139*, 18170−18173.
(23) Ghara, M.; Pan, S.; Chattaraj, P. K. A theoretical investigation on boron-ligand cooperation to activate molecular hydrogen by a frustrated Lewis pair and subsequent reduction of carbon dioxide. *Phys. Chem. Chem. Phys.* **2019**, *21*, 21267−21277.
(24) Ghara, M.; Giri, S.; Chattaraj, P. K. Cycloaddition Reactions between H_2C = CHR (R = H, CN, CH_3) and a Cyclic P/B Frustrated Lewis Pair: A DFT Study. *J. Phys. Chem. A* **2020**, *124*, 4455−4462.
(25) Ghara, M.; Giri, S.; Das, P.; Chattaraj, P. K. Possible C-F bond activation by $B(C_6F_5)_3$/lutidine and $Al(C_6F_5)_3$/lutidine frustrated Lewis pair: an in silico study. *J. Chem. Sci.* **2022**, *134*, 14−26.
(26) Mondal, H.; Ghara, M.; Chattaraj, P. K. A computational investigation of the activation of allene (H_2C = C = CHR; R = H, CH_3, CN) by a frustrated phosphorous/boron Lewis pair. *Chem. Phys. Lett.* **2021**, *774*, 138623−138629.
(27) Ghara, M.; Chattaraj, P. K. A computational study on hydrogenation of CO_2, catalyzed by a bridged B/N frustrated Lewis pair. *Struct. Chem.* **2019**, *30*, 1067−1077.
(28) Ghara, M.; Chattaraj, P. K. Can a decrease in anti-aromaticity increase the dihydrogen activation ability of a frustrated phosphorous/borane Lewis pair? A DFT study. *Theor. Chem. Acc.* **2020**, *139*, 183−189.
(29) Pal, R.; Ghara, M.; Chattaraj, P. K. Activation of Small Molecules and Hydrogenation of CO_2 Catalyzed by Frustrated Lewis Pairs. *Catalysts* **2022**, *12*, 201−230.
(30) Yepes, D.; Jaque, P.; Fernández, I. Deeper Insight into the Factors Controlling H_2 Activation by Geminal Aminoborane-Based Frustrated Lewis Pairs. *Chem.—Eur. J.* **2016**, *22*, 18801−18809.
(31) Yepes, D.; Jaque, P.; Fernández, I. Hydrogenation of Multiple Bonds by Geminal Aminoborane-Based Frustrated Lewis Pairs. *Chem.—Eur. J.* **2018**, *24*, 8833−8840.
(32) Cabrera-Trujillo, J. J.; Fernández, I. Influence of the Lewis Acid/Base Pairs on the Reactivity of Geminal E-CH_2-E' Frustrated Lewis Pairs. *Chem.—Eur. J.* **2018**, *24*, 17823−17831.
(33) Cabrera-Trujillo, J. J.; Fernández, I. Aromaticity can enhance the reactivity of P-donor/borole frustrated Lewis pairs. *Chem. Commun.* **2019**, *55*, 675−678.
(34) Cabrera-Trujillo, J. J.; Fernández, I. Understanding the role of frustrated Lewis pairs as ligands in transition metal-catalyzed reactions. *Dalton Trans.* **2020**, *49*, 3129−3137.
(35) Federmann, P.; Herwig, C.; Beckmann, F.; Cula, B.; Limberg, C. Ring-Opening of THF via an Intramolecular P/Al-Based Frustrated Lewis Pair: Assistance by C_6F_5 Groups beyond Electronegativity? *Organometallics* **2021**, *40*, 4143−4149.
(36) Holschumacher, D.; Bannenberg, T.; Hrib, C. G.; Jones, P. G.; Tamm, M. Heterolytic Dihydrogen Activation by a Frustrated Carbene-Borane Lewis Pair. *Angew. Chem., Int. Ed.* **2008**, *47*, 7428−7432.
(37) Birkmann, B.; Voss, T.; Geier, S. J.; Ullrich, M.; Kehr, G.; Erker, G.; Stephan, D. W. Frustrated Lewis Pairs and Ring-Opening of THF, Dioxane, and Thioxane. *Organometallics* **2010**, *29*, 5310−5319.
(38) Kronig, S.; Theuergarten, E.; Holschumacher, D.; Bannenberg, T.; Daniliuc, C. G.; Jones, P. G.; Tamm, M. Dihydrogen Activation by Frustrated Carbene-Borane Lewis Pairs: An Experimental and Theoretical Study of Carbene Variation. *Inorg. Chem.* **2011**, *50*, 7344−7359.
(39) Wallach, C.; Geitner, F. S.; Fässler, T. F. FLP-type nitrile activation and cyclic ether ring-opening by halo-borane nonagermanide-cluster Lewis acid-base pairs. *Chem. Sci.* **2021**, *12*, 6969−6976.
(40) Föhrenbacher, S. A.; Zeh, V.; Krahfuss, M. J.; Ignat'ev, N. V.; Finze, M.; Radius, U. Tris(pentafluoroethyl) difluorophosphorane and N-Heterocyclic Carbenes: Adduct Formation and Frustrated Lewis Pair Reactivity. *Eur. J. Inorg. Chem.* **2021**, *2021*, 1941−1960.
(41) Mo, Z.; Kolychev, E. L.; Rit, A.; Campos, J.; Niu, H.; Aldridge, S. Facile Reversibility by Design: Tuning Small Molecule Capture and Activation by Single Component Frustrated Lewis Pairs. *J. Am. Chem. Soc.* **2015**, *137*, 12227−12230.
(42) Welch, G. C.; Masuda, J. D.; Stephan, D. W. Phosphonium-Borate Zwitterions, Anionic Phosphines, and Dianionic Phosphonium-Dialkoxides via Tetrahydrofuran Ring-Opening Reactions. *Inorg. Chem.* **2006**, *45*, 478−480.
(43) Chapman, A. M.; Haddow, M. F.; Wass, D. F. Frustrated Lewis Pairs beyond the Main Group: Synthesis, Reactivity, and Small Molecule Activation with Cationic Zirconocene-Phosphinoaryloxide Complexes. *J. Am. Chem. Soc.* **2011**, *133*, 18463−18478.
(44) Frisch, M. J.; Trucks, G. W.; Schlegel, H. B.; Scuseria, G. E.; Robb, M. A.; Cheeseman, J. R.; Scalmani, G.; Barone, V.; Mennucci, B.; Petersson, G. A.; Nakatsuji, H.; Caricato, M.; Li, X.; Hratchian, H. P.; Izmaylov, A. F.; Bloino, J.; Zheng, G.; Sonnenberg, J. L.; Hada, M.; Ehara, M.; Toyota, K.; Fukuda, R.; Hasegawa, J.; Ishida, M.; Nakajima, T.; Honda, Y.; Kitao, O.; Nakai, H.; Vreven, T.; Montgomery, Jr, J. A.; Peralta, J. E.; Ogliaro, F.; Bearpark, M.; Heyd, J. J.; Brothers, E.; Kudin, K. N.; Staroverov, V. N.; Keith, T.; Kobayashi, R.; Normand, J.; Raghavachari, K.; Rendell, A.; Burant, J. C.; Iyengar, S. S.; Tomasi, J.; Cossi, M.; Rega, N.; Millam, J. M.; Klene, M.; Knox, J. E.; Cross, J. B.; Bakken, V.; Adamo, C.; Jaramillo, J.; Gomperts, R.; Stratmann, R. E.; Yazyev, O.; Austin, A. J.; Cammi, R.; Pomelli, C.; Ochterski, J. W.; Martin, R. L.; Morokuma, K.; Zakrzewski, V. G.; Voth, G. A.; Salvador, P.; Dannenberg, J. J.; Dapprich, S.; Daniels, A. D.; Farkas, O.; Foresman, J. B.; Ortiz, J. V.; Morokuma, K.; Farkas, Ö.; Foresman, J. B.; Fox, D. J.*Gaussian 16*, revision C.01; Gaussian, Inc.: Wallingford, CT, 2016.
(45) Lee, C.; Yang, W.; Parr, R. G. Development of the Colle-Salvetti correlation-energy formula into a functional of the electron density. *Phys. Rev. B: Condens. Matter Mater. Phys.* **1988**, *37*, 785−789.

https://doi.org/10.1021/acsomega.2c06194
ACS Omega 2023, 8, 5316−5331

(46) Stephens, P. J.; Devlin, F. J.; Chabalowski, C. F.; Frisch, M. J. J. Ab Initio Calculation of Vibrational Absorption and Circular Dichroism Spectra Using Density Functional Force Fields. *J. Phys. Chem.* **1994**, *98*, 11623−11627.
(47) Weigend, F. Accurate Coulomb-fitting basis sets for H to Rn. *Phys. Chem. Chem. Phys.* **2006**, *8*, 1057−1065.
(48) Grimme, S.; Antony, J.; Ehrlich, S.; Krieg, H. A consistent and accurate ab initio parametrization of density functional dispersion correction (DFT-D) for the 94 elements H-Pu. *J. Chem. Phys.* **2010**, *132*, 154104−154122.
(49) Grimme, S.; Ehrlich, S.; Goerigk, L. Effect of the Damping Function in Dispersion Corrected Density Functional Theory. *J. Comput. Chem.* **2011**, *32*, 1456−1465.
(50) Chen, Y.; Petz, W.; Frenking, G. Is It Possible to Synthesize a Low-Valent Transition Metal Complex with a Neutral Carbon Atom as Terminal Ligand? A Theoretical Study of $(CO)_4FeC$. *Organometallics* **2000**, *19*, 2698−2706.
(51) Yang, M.-C.; Su, M.-D. The Theoretical Investigations of The Reactivity of Neutral Molecules that Feature an M = M (M = B, Al, Ga, In, and Tl) Double Bond. *New J. Chem.* **2019**, *43*, 9364−9375.
(52) Fukui, K. The path of chemical reactions - the IRC approach. *Acc. Chem. Res.* **1981**, *14*, 363−368.
(53) Wolters, L. P.; Bickelhaupt, F. M. The activation strain modeland molecular orbital theory. *WIREs Comput. Mol. Sci.* **2015**, *5*, 324−343.
(54) van Zeist, W. J.; Bickelhaupt, F. M. The activation strain model of chemical reactivity. *Org. Biomol. Chem.* **2010**, *8*, 3118−3127.
(55) Fernandez, I.; Bickelhaupt, F. M. The activation strain model and molecular orbital theory: understanding and designing chemical reactions. *Chem. Soc. Rev.* **2014**, *43*, 4953−4967.
(56) Ess, D. H.; Houk, K. N. Distortion/interaction energy control of 1,3-dipolar cycloaddition reactivity. *J. Am. Chem. Soc.* **2007**, *129*, 10646−10647.
(57) Bickelhaupt, F. M.; Houk, K. N. Analyzing Reaction Rates with the Distortion/Interaction-Activation Strain Model. *Angew. Chem. Int. Ed.* **2017**, *56*, 10070−10086.
(58) Bickelhaupt, F. M. Understanding reactivity with Kohn-Sham molecular orbital theory: E_2- SN_2 mechanistic spectrum and other concepts. *J. Comput. Chem.* **1999**, *20*, 114−128.
(59) Bickelhaupt, F. M.; Baerends, E. J. Kohn- Sham Density Functional Theory: Predicting and Understanding Chemistry. *Rev. Comput. Chem.* **2007**, *15*, 1−86.
(60) te Velde, G.; Bickelhaupt, F. M.; Baerends, E. J.; Fonseca Guerra, C.; van Gisbergen, S. J. A.; Snijders, J. G.; Ziegler, T. Chemistry with ADF. *J. Comput. Chem.* **2001**, *22*, 931−967.
(61) Diefenbach, A.; de Jong, G. T.; Bickelhaupt, F. M. Activation of H-H, C-H, C-C and C-Cl Bonds by Pd and $PdCl^-$. Understanding Anion Assistance in C-X Bond Activation. *J. Chem. Theory Comput.* **2005**, *1*, 286−298.
(62) Mitoraj, M. P.; Michalak, A.; Ziegler, T. A. A Combined Charge and Energy Decomposition Scheme for Bond Analysis. *J. Chem. Theory Comput.* **2009**, *5*, 962−975.
(63) Mitoraj, M.; Michalak, A. Natural Orbitals for Chemical Valence as Descriptors of Chemical Bonding in Transition Metal Complexes. *J. Mol. Model.* **2007**, *13*, 347−355.
(64) Mitoraj, M.; Michalak, A. Donor-acceptor properties of ligands from the natural orbitals for chemical valence. *Organometallics* **2007**, *26*, 6576−6580.
(65) Michalak, A.; Mitoraj, M.; Ziegler, T. Bond orbitals from chemical valence theory. *J. Phys. Chem. A* **2008**, *112*, 1933−1939.
(66) Mitoraj, M.; Michalak, A. Applications of natural orbitals for chemical valence in a description of bonding in conjugated molecules. *J. Mol. Model.* **2008**, *14*, 681−687.
(67) von Hopffgarten, M.; Frenking, G. Energy decomposition analysis. *Wiley Interdiscip. Rev.: Comput. Mol. Sci.* **2012**, *2*, 43−62.
(68) Zhao, L. L.; von Hopffgarten, M.; Andrada, D. M.; Frenking, G. Energy decomposition analysis. *Wiley Interdiscip. Rev.: Comput. Mol. Sci.* **2018**, *8*, No. e1345.
(69) Zhang, Z.-F.; Yang, M.-C.; Su, M.-D. Significant Insight Into the Origin of Reaction Barriers Determining Dihydrogen Activation by G13-P-P (G13 = Group 13 Element) and G15-P-Ga (G15 = Group 15 Element) Frustrated Lewis Pairs. *Inorg. Chem.* **2021**, *60*, 15253−15269.
(70) Yang, M.-C.; Zhang, Z.-F.; Su, M.-D. Insights Into the Factors Controlling the H-H bond Cleavage Reactions by Five-Membered G13/P (G13 = Group 13 Element) and B/G15 (G15 = Group 15 Element) Frustrated Lewis Pairs. *Organometallics* **2022**, *41*, 374−389.
(71) van Lenthe, E.; Ehlers, A.; Baerends, E. J. Geometry optimizations in the zero order regular approximation for relativistic effects. *J. Chem. Phys.* **1999**, *110*, 8943−8053.
(72) van Lenthe, E.; Baerends, E. J. Optimized Slater-type basis sets for the elements 1−118. *J. Comput. Chem.* **2003**, *24*, 1142−1156.
(73) *Computer code ADF2017, SCM, Theoretical Chemistry*; Vrije Universiteit: Amsterdam, http://www.scm.com.
(74) Fischer, E. O.; Maasböl, A. Zur Frage eines Wolfram-Carbonyl-Carben-Komplexes. *Angew. Chem.* **1964**, *76*, 645.
(75) Schrock, R. R. High Oxidation State Multiple Metal-Carbon Bonds. *Chem. Rev.* **2002**, *102*, 145−180.
(76) After we submitted this article, one reviewer suggested that the HOMO/LUMO of the FLP-type system should weakly interact before the small molecule is placed in between. This type of FLP preinteraction can be found here: Heshmat, M.; Privalov, T. H_2 Cleavage by Frustrated Lewis Pairs Characterized by the Energy Decomposition Analysis of Transition States: An Alternative to the Electron Transfer and Electric Field Models. *J. Phys. Chem. A* **2018**, *122*, 7202−7211.
(77) We used the B3LYP-D3(BJ)/def2-TZVP method to optimize these reactant molecules (**G13/P-Rea**) and then used the vibrational frequency calculation to prove that they have no imaginary frequency. This means that these reactant structures we calculated are at the minimum of energy. Furthermore, we tried to calculate other possible structural conformations of **G13/P-Rea**. However, the energies of these other conformations and true minimum energies of **G13/P-Rea** were found to be about 1.04−5.15 kcal/mol higher. Therefore, we believe that all optimized structures of **G13/P-Rea** given in Figure 3 are at the global minima. Then, we calculated the lengths of G13(LA) and P(LB) of **G13/P-Rea** by using Cartesian coordinates of G13 and P atoms in the optimized structures of **G13/P-Rea**. As a result, we can readily obtain the G13···P separating distance in **G13/P-Rea**, whose data are already shown in Figure 3. See the Supporting Information.
(78) The atomic radii of group 13 element increase in the order B (84 pm) < Al (121 pm) < Ga (122 pm) < In (142 pm) < Tl (145 pm). See ref 79.
(79) Cordero, B.; Gómez, V.; Platero-Prats, A. E.; Revés, M.; Echeverría, J.; Cremades, E.; Barragán, F.; Alvarez, S. Covalent radii revisited. *Dalton Trans.* **2008**, *37*, 2832−2838.
(80) Similar to Figure 3, we also used the B3LYP-D3(BJ)/def2-TZVP method to obtain the true global minima of the **Al/G15-Rea** molecules. Then, using Cartesian coordinates of Al(LA) and G15(LB) in the optimized structure of **Al/G15-Rea**, we can obtain the separating distance between Al and G15 atoms, whose data are all collected in Figure 4. See the Supporting Information.
(81) According to a calculation work reported by Limberg and co-workers,[35] the energy difference between the transition state and the final product was predicted to be 34.8 kcal/mol. In addition, this calculated energy value was based on the single-point DLPNO-CCSD(T)/Def2-TZVP//B3LYP-D3/def2-SVP level and the solvent effect. However, our B3LYP-D3(BJ)/def2-TZVP results shown in Figure 4 indicated that the calculated free energy between the transition state (**Al/P-TS**) and the final product (**Al/P-Prod**) was predicted to be 31.4 kcal/mol, which is based on the gas phase. From these comparisons, we are confident that our theoretical data should be reliable. See the Supporting Information.
(82) We used the results of the optimized structures of transition states **Al/G15-TS** in Figure 4. That is, the separating distance between the two atoms of Al(LA) and G15(LB) in **Al/G15-TS** (the Al···G15 distance can be obtained using Cartesian coordinates of **Al/G15-TS**) is set up as the *x* axis, and the corresponding free energy barrier of **Al/G15-TS** calculated at the B3LYP-D3(BJ)/def2-TZVP level is set up as

https://doi.org/10.1021/acsomega.2c06194
ACS Omega 2023, 8, 5316−5331

the *y* axis. Then, the straight line graph shown in Figure 5 can be readily obtained. See the Supporting Information.

(83) Fukui, K. Recognition of stereochemical paths by orbital interaction. *Acc. Chem. Res.* **1971**, *4*, 57−64.

(84) Li, Z.; Chen, X.; Andrada, D. M.; Frenking, G.; Benkö, Z.; Li, Y.; Harmer, J.; Su, C.-Y.; Grützmacher, H. $(L)_2C_2P_2$: Dicarbondiphosphide Stabilized by N-Heterocyclic Carbenes or Cyclic Diamido Carbenes. *Angew. Chem., Int. Ed.* **2017**, *56*, 5744−5749.

(85) Heshmat, M.; Ensing, B. Optimizing the Energetics of FLP-Type H_2 Activation by Modulating the Electronic and Structural Properties of the Lewis Acids: A DFT Study. *J. Phys. Chem. A* **2020**, *124*, 6399−6410.

(86) The activation energy surface $\Delta E_{ACT}(\gamma)$ is decomposed, along the reaction coordinate γ, into the deformation energy $\Delta E_{DEF}(\gamma)$ associated with the structural deformation that the reactants undergo and the interaction $\Delta E_{INT}(\gamma)$ between these increasingly deformed reactants. As a result, $\Delta E_{ACT}(\gamma) = \Delta E_{DEF}(\gamma) + \Delta E_{INT}(\gamma) = [\Delta E_{DEF,THF}(\gamma) + \Delta E_{DEF,G13/G15\text{-}Rea}(\gamma)] + \Delta E_{INT}(\gamma)$. It is the interplay between $\Delta E_{DEF}(\gamma)$ and $\Delta E_{INT}(\gamma)$ that determines if and at which point along γ a barrier arises. This decomposition of the energy $\Delta E_{ACT}(\gamma)$ is carried out along the intrinsic reaction coordinate (IRC), provided by the IRC method as discussed in ref 52, that is to say, from the separate reactants (or from a weakly bonded reactant complex when it exists) to the reaction products via the corresponding transition state. In this work, to be able to well explain the main factor that really affects the activation energy when breaking the THF ring, we choose the C−O bond elongation of THF as the reaction coordinate. When the C−O bond length is extended every 0.05 Å, a new geometric structure is obtained and then the IRC calculation is made once. Then, the calculated $\Delta E_{ACT}(\gamma)$, $\Delta E_{DEF,THF}(\gamma)$, $\Delta E_{DEF,G13/G15\text{-}Rea}(\gamma)$, and $\Delta E_{INT}(\gamma)$ corresponding to each geometric point can be plotted as a function of the C−O bond length, which is shown in Figures 11 and 13.

https://doi.org/10.1021/acsomega.2c06194
ACS Omega 2023, 8, 5316−5331